Missouri S&T Library and Learning Resources

Scholars' Mine

Doctoral Dissertations | Student Theses and Dissertations

1968

The damage assessment of thermally shocked high density, high purity aluminum oxide

John H. Ainsworth

Follow this and additional works at: https://scholarsmine.mst.edu/doctoral_dissertations

 Part of the Ceramic Materials Commons

Department: Materials Science and Engineering

Recommended Citation

Ainsworth, John H., "The damage assessment of thermally shocked high density, high purity aluminum oxide" (1968). *Doctoral Dissertations*. 1916.
https://scholarsmine.mst.edu/doctoral_dissertations/1916

This thesis is brought to you by Scholars' Mine, a service of the Missouri S&T Library and Learning Resources. This work is protected by U. S. Copyright Law. Unauthorized use including reproduction for redistribution requires the permission of the copyright holder. For more information, please contact scholarsmine@mst.edu.

THE DAMAGE ASSESSMENT OF THERMALLY SHOCKED HIGH DENSITY, HIGH PURITY ALUMINUM OXIDE

by

John H. Ainsworth

A

THESIS

submitted to the faculty of the

UNIVERSITY OF MISSOURI-ROLLA

in partial fulfillment of the requirements for the

Degree of

DOCTOR OF PHILOSOPHY IN CERAMIC ENGINEERING

Rolla, Missouri

1968

Approved by

Robert C. Evans (Advisor) _____

Delbert E. Day _____

Lee J. Bain

R.L. Davis _____

_____

ABSTRACT

The traditional approach to thermal shock testing in brittle materials has been to determine the temperature difference required to nucleate cracks in these materials. Recent work has indicated that the degree of damage after crack nucleation should be an additional consideration. The degree of damage resulting from cooling thermal shocks has been the primary consideration of the present work. Test specimens of two geometries: long, solid rods and short, solid cylinders were quenched from selected temperatures into ice water. The degree of damage was determined through strength measurements and sonic damping analysis. Initial damage occurred at a temperature difference above 150°C; this was characterized by significant decreases in strength, increases in strength data dispersion, and changes in sonic behavior. A model has been employed to predict degree of damage using crack depths as a criteria. Good agreement is seen between the predicted crack depths and observed crack depths at low temperature differences. At higher temperature differences, crack densities increase, and crack interactions affect the agreement between the predicted crack depths and those observed.

ACKNOWLEDGEMENTS

The author wishes to express his sincere gratitude to his advisor, Dr. Robert E. Moore, for his support and encouragement.

The helpful discussions with Dr. Thomas S. Montgomery are also acknowledged.

The financial assistance of the National Science Foundation and Kaiser Aluminum and Chemical Corporation in the form of fellowships and research funds is acknowledged and greatly appreciated.

I should also like to thank my wife, Alice, without whose aid and understanding, the work would not have been completed.

TABLE OF CONTENTS

	Page
ABSTRACT	ii
ACKNOWLEDGEMENTS	iii
LIST OF FIGURES	vi
LIST OF TABLES	viii
I. INTRODUCTION	1
II. REVIEW OF LITERATURE	3
A. Determination of Maximum Temperature Difference a Body Can Withstand	3
1. Unsteady State: Infinite Heat Transfer Coefficient	5
2. Unsteady State: Finite Heat Transfer Coefficient	5
3. Steady State	5
4. Constant Heating or Cooling Rate	6
5. Radiation Heating and Cooling	6
B. Effect of Material Properties on ΔT_{max}	7
C. Degree of Damage After Crack Initiation	10
D. Methods of Thermal Shock Testing	13
III. TEST PROCEDURES	15
A. Material and Test Specimens	15
B. Thermal Shock Techniques	15
1. Heating and Cooling Shock Treatment	15
2. Cooling Shock Treatment	16
C. Strength Determinations	17
1. Short Cylinders	17
2. Bend Tests	18
D. Determination of Young's Modulus of Elasticity	18
E. Logarithmic Decrement Determinations	20
F. Surface Decoration Techniques	24
G. Determination of Heat Transfer Coefficient	25
IV. RESULTS	27
A. Strengths of Short Cylinders	27
B. Strengths of Long Rods	31

Page

C. Elastic and Anelastic Properties of Long Rods 36
D. Crack Characteristics of Long Rods 36

1. Crack Densities 36
2. Crack Depths 43

V. DISCUSSION 46

A. General Analysis of Measurements on Short Cylinders 46
B. General Analysis of Measurements on Long Rods 47
C. Comparison of Strength Measurements of Rods and Cylinders 50
D. Predictions of Damage in Terms of Crack Depths 51
E. Agreement Between Theory and Experiment for Crack Initiation 58
F. Discussion of Thermal Shock Techniques 60

VI. SUMMARY AND CONCLUSIONS 62

VII. RECOMMENDATIONS FOR FUTURE WORK 64

BIBLIOGRAPHY 65
APPENDIX A: Letter Symbols 69
APPENDIX B: Stress Distribution in Long Solid Cylinders 73
APPENDIX C: Cooling Curves for Determining the Heat Transfer Coefficient 74
APPENDIX D: Material Properties and Sample Calculations 78
VITA 90

LIST OF FIGURES

Figure		Page
1.	Schematic of sonic apparatus	19
2.	Frequency-phase set-up	22
3.	Lissajous figure orientations	23
4.	Strengths of short cylinders as a function of temperature difference	28
5.	Strength data dispersions of short cylinders	29
6.	Strength decreases in short cylinders as a function of thermal shock cycles	32
7.	Strengths of long rods as a function of temperature difference	34
8.	Strength data dispersions of long rods	37
9.	Elastic modulus as a function of shock temperature difference	39
10.	Internal friction as a function of shock temperature difference	40
11.	Crack densities as a function of thermal shock level	42
12.	Crack depths resulting from thermal shock	44
13.	Relationship between $\Gamma(d/b)$ and d/b	53
14.	Stress distribution in tangential direction at 175°C	55
15.	Predicted and observed crack depths	56
16.	Cooling curves used to determine surface heat transfer coefficient	75
17.	Cooling curves plotted in terms of dimensionless temperature and dimensionless time	76
18.	Thermal conductivity dependence on temperature of Al_2O_3	79
19.	Thermal expansion of Al_2O_3	79

20. Temperature dependence of strength of Al_2O_3 80

21. Temperature dependence of Young's modulus of Al_2O_3 80

22. The effect of property evaluation temperature on the calculated ΔT_{max} 83

23. Graphical method for calculating crack depths ... 89

LIST OF TABLES

Table		Page
I.	Strength Data on Short Cylinders	30
II.	Strengths of Short Cylinders after Cycling	33
III.	Strength Data on Long Rods	35
IV.	Modulus of Elasticity and Logarithmic Decrement	38
V.	Crack Densities in Long Rods	41
VI.	Crack Depths in Long Rods	45
VII.	Normalized Stress Edge Intensity Factors	53
VIII.	Dimensionless Tangential Stresses at the Time of Maximum Stress as a Function of Dimensionless Radial Coordinates and Biot's Modulus ..	82
IX.	Effects of Property Evaluation Temperature on Calculated ΔT_{max}	84
X.	Calculations for Tangential Crack Depths Resulting From 175°C ΔT Shock	87

I. INTRODUCTION

Thermal shock resistance is not an intrinsic property of brittle materials; it depends upon the thermal and physical characteristics of the system being considered. Definitions relating to the term thermal shock resistance are varied; however, a general definition is: the resistance of a part to damage resulting from intensive stresses arising through sudden temperature differences within a body.

Within the last two decades, thermal shock has become a matter of increased concern, particularly in the aerospace field. The high temperatures encountered in high-performance, high-velocity military and space vehicles suggest the use of ceramic materials; however, brittle nature and poor thermal shock resistance have severely limited their use. This is true particularly in components exposed to extremely rapid heating, such as nose cones, leading edges, and rocket nozzles.

The aerospace field is by no means the only area concerned with thermal shock. In the steel industry, refractory linings in smelting furnaces are subject to spalling or the breaking away of small fragments of material; a direct result of thermal shock.

In the past, the approach to thermal shock testing in the laboratory has involved determining the temperature difference, ΔT, required to initiate fracture. Although

periodically discussed, little effort has been directed toward the determination of damage after fracture initiation. During the past five years, attempts[1] have been made to predict the degree of damage incurred during rapid heat-up shocks; yet little work has been done to characterize damage on cooling.

This investigation is an effort to evaluate the damage to high purity, high density Al_2O_3 resulting from cooling shocks. The experimental approach to characterizing data in this work included:

a) direct strength deterioration measurements,

b) surface crack detection and characterization,

c) changes in acoustic damping, and

d) statistics of strength data.

A model is presented to explain the damage on cooling, and deviations from this model are examined.

II. REVIEW OF LITERATURE

Hummel[2] has stated that it is very difficult to define a thermal shock resistant ceramic except to say that it is a composition which does not fail under the thermal stress which is developed during some stated temperature cycling process. One must at least specify the conditions of testing and the size and shape of the body being tested before any estimate can be made of the probable performance of any given ceramic body with respect to thermal shock resistance.

In present thinking, an evaluation of the thermal shock resistance of a brittle material may be divided into two parts:

1. The determination of the maximum temperature difference a body can withstand without crack initiation.
2. The degree of damage incurred by a body after cracks have been initiated.

A. Determination of Maximum Temperature Difference a Body Can Withstand

The first equation relating material properties to the maximum temperature difference a body can tolerate is attributed to Winkelman and Schott[3]. These investigators used glass compositions, tested them over a very limited range, and proposed the following relationship between maximum temperature difference and certain physical

properties:

$$\Delta T = \frac{\sigma k}{E\alpha}, \tag{1}$$

where σ = tensile strength of material,

k = thermal conductivity,

E = Young's Modulus of Elasticity, and

α = linear coefficient of thermal expansion.

A glossary of terms and units assigned to these terms is given in Appendix A.

Many "thermal shock factors" are found in the literature[4,5,6,7] which relate directly or indirectly to ΔT_{max}. These factors are expressed in terms of material properties, and are used to give relative indications of the thermal shock resistance of brittle materials. Examples are:

$$R \equiv \frac{\sigma(1-\mu)}{E\alpha}, \tag{2}$$

$$R' \equiv \frac{\sigma(1-\mu)k}{E\alpha}, \tag{3}$$

$$R'' \equiv \frac{\sigma(1-\mu)a}{E\alpha}, \tag{4}$$

$$R_{rad} \equiv \left[\frac{\sigma(1-\mu)k}{\alpha E\epsilon}\right]^{1/4}, \tag{5}$$

where μ = Poisson's ratio,

a = thermal diffusivity,

ϵ = emissivity, and

R, R', R'', and R_{rad} are thermal shock resistance factors. The applicability of the above factors are shown in the

following five cases. The first four cases are discussed by Kingery[4], while Hasselman[5] has reported in detail on the fifth case.

1. Unsteady State: Infinite Heat Transfer Coefficient

In this case, the heat transfer coefficient is so large that a body, originally at T_0, when quenched to T_1 will have its surface at T_1 and its interior at T_0. The maximum temperature difference under these conditions is:

$$\Delta T_{max} = R \cdot S, \tag{6}$$

where S is a shape factor taking into account both size and shape.

2. Unsteady State: Finite Heat Transfer Coefficient

This case, while relatively simple, is considered to approximate many actual problems. The maximum temperature difference is given by:

$$\Delta T_{max} = R' \cdot S \cdot \frac{1}{h}, \tag{7}$$

where h = heat transfer coefficient.

3. Steady State

The steady state temperature distribution depends on the thermal conductivity and on the rate of heat flow, q, per unit area. For any given sample, if S is a shape factor and ΔT is the overall temperature difference:

$$q = -kS\Delta T \tag{8}$$

and the conditions are uniquely defined by specifying

either the heat flow or the temperature difference:

$$\Delta T = R \cdot S, \tag{9}$$

$$q_{max} = R' \cdot S.$$

4. Constant Heating or Cooling Rate

If a constant rate of temperature change, θ°/sec., is maintained on the surface of the body, the maximum rate of temperature change without fracture is given by:

$$\theta_{max} = R'' \cdot S. \tag{10}$$

5. Radiation Heating and Cooling

The maximum temperature achieved through direct radiation to which a body with low initial temperature can be subjected is:

$$T_{max} = \left[\frac{S}{\rho}\right]^{1/4} \cdot R_{rad}, \tag{11}$$

where ρ = density.

Although only an approximation, equation 11 can be used to estimate the ΔT_{max} to which a body can be cooled by radiation.

Analytical solutions of thermal stress problems for simple shapes and known heat transfer conditions have been presented by various investigators[8,9,10]. These give solutions to the various problems in terms of dimensionless parameters evaluated as a function of time, space coordinates, and heat transfer conditions. From such solutions,

the shape factor S can be determined. Appendix B gives the equations dealing with a long circular cylinder as presented by Jaeger[8].

Several approximate shape factors have also been suggested by various authors[11,12,13]. These shape factors are applicable to surface stresses; they are for relatively low heat transfer coefficients, such as found in gas convection and radiation cooling. Kingery[4] has listed these approximations as:

$$S \simeq 4/\beta \qquad \text{after Bradshaw}^{11}, \qquad (12)$$

$$S \simeq 4/\beta + 1 \qquad \text{after Buessem}^{12}, \text{ and} \qquad (13)$$

$$S \simeq 3.25/\beta \qquad \text{after Manson}^{13}. \qquad (14)$$

Here, β is Biot's modulus, $\frac{hx}{k}$,

where x = the half thickness or radius of the body.

B. Effect of Material Properties on ΔT_{max}

The various relationships given previously show in what manner material properties affect the maximum ΔT. Thus, for a given set of heat transfer conditions, one should look for a material with high strength, high thermal conductivity, low Poisson's ratio, low thermal expansion, and low elastic modulus. In almost every case, meeting the above criteria simultaneously is impossible because, for example, brittle materials with high strengths also exhibit high elastic moduli. These properties work against one another in thermal shock conditions.

In addition to the material properties discussed above, many other characteristics of the body must be considered. The effect of porosity on ΔT_{max} has been studied by Kingery and Coble[14]. Specimens with controlled porosity were prepared by incorporating napthalene flakes in an alumina casting slip. By preparing and firing specimens under controlled conditions so that the continuous solid phase was consistent in structure, the effect of porosity could be accurately observed. It was found that the maximum temperature difference decreases with increasing porosity. ΔT_{max} for a sample with 50% porosity was about 1/3 that for fully dense samples.

Kingery and Coble[15] have reviewed the effect of grain size on the strengths of brittle materials. Decreases in strength are noted with increasing grain size. Large grain size would thus have an adverse effect on thermal shock resistance. It is reported[15] that above 95% theoretical density, the change in grain size is the most important strength variable. The strengths of alumina samples, having densities in this range, varied from 70-80,000 psi at 1μ grain size down to 20,000 psi at about 100μ.

Hasselman[5], in his analysis of radiation thermal shock, has discussed the role of emissivity. The lower the emissivity, the higher the shock resistance. Hasselman points out that surface conditions play an important role, and smooth polished surfaces are desired for optimum shock

resistance.

It has been suggested[2,16,17] that anisotropy plays an important role in governing the thermal shock resistance of a brittle material. Consider two crystals lying side by side, each oriented in a different crystallographic direction. A large difference in thermal expansion would set up severe shear stresses across the grain boundaries, and these stresses could conceivably nucleate cracks.

A situation analogous to anisotropy exists in polyphase ceramics wherein two or more phases are present and each phase has different properties. An attempt to estimate the order of stresses which may arise in a two-phase material in which the thermal expansion coefficients of the two phases differ has been made by Kingery[18]. Kingery considers one phase to be dispersed as discrete particles in a continuous matrix of the other. If no separation between the phases due to thermal expansion occurs, Turner[19] has shown that the average thermal expansion coefficient should be given by:

$$\alpha = \frac{\alpha_1 p_1 K_1 + \alpha_2 p_2 K_2}{\frac{p_1 K_1}{\rho_1} + \frac{p_2 K_2}{\rho_2}}, \qquad (15)$$

where p_1, p_2 = weight fractions of phases,

K_1, K_2 = bulk moduli of phases, and

ρ_1, ρ_2 = densities of phases.

Assuming that the stresses set up due to a change in temperature from T_0 to T_1 are entirely elastic, the stresses

in phase one should be given by[18]:

$$\sigma_1 = (\alpha - \alpha_1)(T - T_0)K_1. \qquad (16)$$

Using this formula, Kingery estimated that stresses set up in a silica glass containing 10% cristobalite after cooling from 1200°C would be of the order of one million psi. Stresses of that order would readily cause cracking.

The considerations given previously for ΔT_{max} indicate that crack initiation occurs when a definite critical stress is reached. Manson and Smith[20] have proposed a theory of thermal shock resistance based on Weibull's[21] statistical theory of strength. Brittle materials do not obey a criterion where fracture occurs on the achievement of a definite critical stress. Weibull has developed a statistical theory to account for this behavior. Manson and Smith, employing Weibull's theory, postulate that fracture most probably occurs not at the time when the surface stress is a maximum, but at a later time when the surface stress has fallen somewhat and a greater volume of material in the interior of the body has been brought up to a moderate stress level.

C. Degree of Damage After Crack Initiation

The discussion up to this point has dealt with the nucleation of fracture, and the material properties which influence this nucleation. Although mechanical failure criteria were recognized and discussed in connection with thermal shock[4,16], no attempts were made to apply these

criteria to damage after crack initiation until Hasselman's[1] work was published.

A criteria for crack propagation or crack nucleation is provided by Griffith[22] who states that a crack will start propagating and continue propagating while the elastic energy released from the stress field surrounding the crack is equal to or greater than the energy necessary to supply the effective surface energy. Those mechanisms making up the effective surface energy are:

a) the thermodynamic free energy,

b) energy dissipation in anelastic deformation at the tip of the propagating crack, and

c) energy dissipated in plastic deformation of a thin layer on the newly formed crack surfaces.

Considering a spherical shape, and assuming that the sphere is shocked by heating from a lower temperature to a higher temperature, Hasselman developed an expression yielding the total elastic energy stored at fracture to be:

$$W = \frac{4\pi x^3 \sigma^2 (1 - \mu)}{7E}. \qquad (17)$$

Hasselman then equated the total surface energy required for the propagation of cracks to the elastic energy stored at fracture. The mean area A over which N number of cracks will then propagate in a sphere is given by:

$$A = \frac{2\pi\sigma^2 (1 - \mu) x^3}{7NE\gamma_{eff}}, \qquad (18)$$

where γ_{eff} = effective surface energy.

Hasselman then defined two additional thermal shock resistance parameters.

$$R''' = \frac{E}{\sigma^2(1 - \mu)}, \text{ and} \tag{19}$$

$$R'''' = \frac{E\gamma_{eff}}{\sigma^2(1 - \mu)}. \tag{20}$$

Since the relative degree of damage will be proportional to the area over which the cracks will propagate, minimizing the quantity A in equation 18 will result in maximum thermal shock damage resistance. This will require low values of strength and high values of Poisson's ratio, Young's modulus of elasticity, and effective surface energy. It will be noted that these values are diametrically opposed to those values required for a high fracture nucleation ΔT. Thus, one is faced with the problem of deciding which is more critical for a given application: the high ΔT or the low degree of damage.

Hasselman's work in this area was fairly well received for it prompted several investigations[23,24] into various facets of this problem. Nakayama and Ishizuka[23] provided experimental evidence that Hasselman's relations were valid and useful. Taking five brands of commercial firebrick, these investigators found that the relative degrees of damage predicted by Hasselman's equations were in agreement with those found by experimentally shocking firebrick.

D. Methods of Thermal Shock Testing

Various types of thermal shock tests are employed to get an indication of the thermal shock resistance of brittle materials. Mohr[25] constructed a furnace for radiant thermal shock testing. The furnace consisted of a chamber five inches on a side through which six one-half inch diameter silicon carbide heating elements pass. The elements are in two horizontal rows of three elements each, at right angles to each other on one and one-half inch centers. A three and one-half inch diameter hole leads from the heating chamber to the furnace top. The material to be tested is in the form of a flat plate. This plate is placed directly on the furnace opening and is exposed to the radiation from the heating elements. The time to fracture is recorded and is used as an indication of the thermal shock resistance.

Baroody, et. al.[26] constructed an apparatus designed to provide a controlled, measurable, heat flow through the wall of a hollow cylindrical specimen. It consisted of a graphite resistor rod in an evacuated chamber. The walls were water cooled and windows were provided for viewing the specimen during testing. The specimen is aligned concentrically around the heater rod between one or more upper and lower guard tubes. Upon applying power to the rod, heat flows rapidly through the specimen, inducing a radial temperature gradient and resultant thermal stresses. The temperature at which a crack is

first observed was used as an indication of thermal shock resistance.

Quenching media are commonly used in thermal shock testing[27,28,29]. Crandall and Ging[27] used Hitec heat transfer salt as a media for heat shocking alumina spheres. By lowering the temperature of the heat transfer salt and raising the initial temperature of the specimens, cooling shocks were also achieved. These investigators also used air moving at a given velocity for cooling shocks. The magnitudes of temperature difference over the ranges in which fracture occurred were studied, and ΔT values were assigned where 50% of the specimens failed.

III. TEST PROCEDURES

A. Material and Test Specimens

The material selected for this study was 99.5% pure Al_2O_3 supplied by Western Gold and Platinum Company. As determined from mass and dimensions, this material had a density of 3.83 ± 0.03 gm/cc. The material was received as six-inch rods having a diameter of one-half inch. The rods were centerless ground to tolerances of ± 0.003 inches in diameter.

Test specimens were of two types: the as-received rods and short solid cylinders, one-half inch by one-half inch, which were cut from the long rods using a diamond saw.

B. Thermal Shock Techniques

Thermal shocking of both short cylinders and long rods was achieved in the following manner:

1. Heating and Cooling Shock Treatment

One group of short cylinders was subjected to both heating and cooling cycles. A container filled with Hitec* heat transfer salt was placed in a Harrop kanthal-heated box furnace. This furnace was heated to a pre-selected temperature between 150°C and 500°C. Upon reaching the holding temperature, the temperature of the heat transfer salt was checked with a calibrated chromel-alumel thermocouple.

Specimens initially at room temperature were immersed

* manufactured by E. I. duPont de Nemours and Co., Inc.

in the Hitec and allowed a ten minute soak. The test pieces were small in relation to the heat bath, and it is felt that the cold specimens did not act to lower the temperature of the heat bath. After soaking, the specimens were removed from the Hitec and quickly immersed in ice water. The ice bath was stirred immediately before the specimens were immersed. Thus, static higher temperature water layers on the surfaces of the test specimens were minimized. When cold, the specimens were dried at 105°C and placed in a desiccator for a period of three days prior to strength testing. Generally, five specimens were shocked at each temperature.

2. Cooling Shock Treatment

This treatment was similar to the double shock described previously; however, in this case, the heat shock was eliminated. Both short cylinders and long rods were subjected to this type of shock. Here the test samples, again consisting of five specimens, were placed in the cold Harrop furnace along with the container of Hitec. The furnace was then heated at a rate of 5°C/min. to the selected temperature between 150°C and 500°C. Upon reaching temperature, the heat transfer bath was checked with a calibrated chromel-alumel thermocouple and the specimens were placed in the bath to insure the same flux to all specimens. After a ten minute soak, the specimens were immersed in ice water, dried, and stored in a desiccator for three days. The temperature

differences to which test specimens were subjected are believed accurate to ±5°C.

C. Strength Determinations

1. Short Cylinders

Strength determinations on short cylinders were made by using the diametral compression technique. This technique has been described elsewhere in detail[30]. The test specimen is placed between two platens in such a manner that compression of the cylinder occurs along a diameter. This generates a fairly uniform tensile stress perpendicular to the diametral plane. The maximum tensile stress developed across a diametral plane in this test is given by:

$$\sigma = \frac{2P}{\pi DL}, \tag{21}$$

where P = load,

L = length, and

D = diameter.

A Tinius-Olsen hydraulic-type testing machine with a low scale range of 30,000 pounds, scale divisions of 50 pounds, was used for testing the short cylinders. If the load is not applied uniformly in this test, incorrect values for strength may be obtained. To insure that errors of this nature were minimized, heavy paper was placed between the specimen and the platens at the lines of contact. After testing, an impression remained on the paper showing where the force was applied. If the impression was uneven,

a non-uniform force was indicated and the strength value was thrown out.

2. Bend Tests

A four-point bend jig was used to determine the bend strengths of the long circular rods. This jig was specially designed so that the specimen contact points consisted of sleeves on ball bearings to reduce frictional effects. The span of maximum tension of this jig was four inches, while the overall span of the jig was six inches. Bend strengths for the circular bars were calculated by use of:

$$\sigma = \frac{16P}{\pi D^3}. \qquad (22)$$

A Tinius-Olsen hydraulic-type universal testing machine with a lowest scale range of 1200 pounds and scale divisions of one pound was used in conjunction with this jig.

D. Determination of Young's Modulus of Elasticity

The dynamic modulus of elasticity was determined on the six-inch rods before and after shocking using sonic apparatus marketed by Electro Products Laboratories Inc. A schematic is shown in Figure 1. This equipment consisted of a Hewlett Packard wide range oscillator used through a power amplifier to drive a Jensen speaker modified to serve as a drive unit to vibrate the rods. The response of the test piece was picked up by an Astatic phonograph cartridge; the relative intensity of the amplified output was then indicated on a D. C. microammeter. The input to

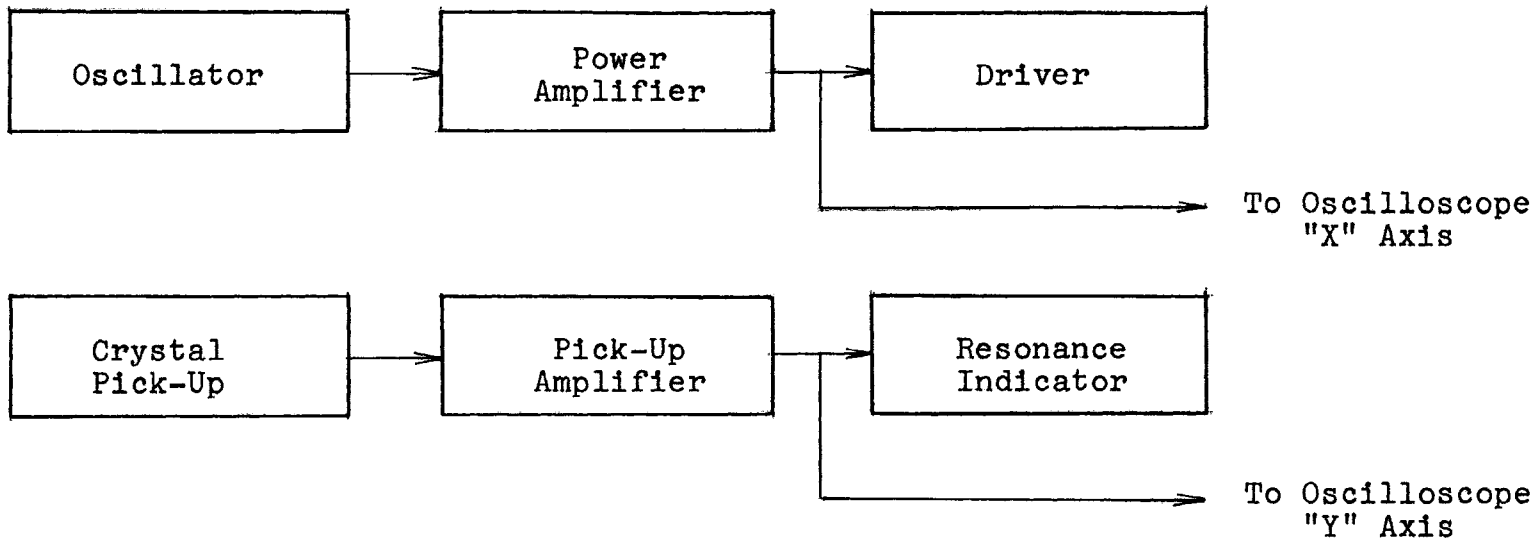

Figure 1. Schematic of sonic apparatus.

the driver and the output of the pick-up were fed into a Fairchild oscilloscope so that resonance frequencies could be determined by use of Lissajous figures on the cathode ray tube. Resonance frequencies were read from a Beckman counter.

The specimens were suspended from the driver and pick-up with nylon thread. The threads were secured close to the specimen nodes (0.224 L where L is the length) for flexural vibration. The frequency was varied until the microammeter and Lissajous figures indicated the specimen to be vibrating in resonance. Young's modulus was then calculated from the specimen dimensions, mass, and the resonance frequency with the aid of tables compiled by Hasselman[31]. The equation used for calculating the E-modulus is:

$$E = Cwf^2. \qquad (23)$$

Here, C = a constant,

w = specimen weight, and

f = resonance frequency.

E. Logarithmic Decrement Determinations

Concurrent with Young's modulus of elasticity, the logarithmic decrement was also determined on the long rods. The technique, called the frequency-phase method, is relatively new and was introduced by Smith and Berns[32]. The author has used this technique previously and has found it quite satisfactory.

Figure 2 shows the general test set-up for the frequency-phase determinations of logarithmic decrement. The input voltages to the oscilloscope are:

$$e_h = C_1 \sin \omega t \qquad \text{horizontal input} \qquad (24)$$

$$e_v = C_2 \sin(\omega t - \phi) \qquad \text{vertical input} \qquad (25)$$

where C_1 and C_2 are the amplitudes of the horizontal and vertical inputs, respectively.

At resonance, the output of the crystal pick-up is 90 degrees ($\pi/2$) out of phase with the output of the driver, and the Lissajous pattern on the oscilloscope is vertical as shown in Figure 3a. If the exciting frequency (f) of the driver is changed slightly, the Lissajous figure is changed slightly as shown in Figure 3b. From Figure 3b and equations 24 and 25 it is apparent that when $\omega t = 0$, or multiples of π, the distance $Y_1/2$ is:

$$Y_1/2 = e_v = C_2 \sin(-\phi). \qquad (26)$$

Likewise, when $\omega t - \phi$ is $\pi/2$, or odd multiples, the distance $Y_2/2$ is:

$$Y_2/2 = C_2. \qquad (27)$$

From equations 26 and 27, the absolute value for sin ϕ is found to be:

$$\text{Sin } \phi = \frac{Y_1/2}{C_2} = Y_1/Y_2 \text{ or} \qquad (28)$$

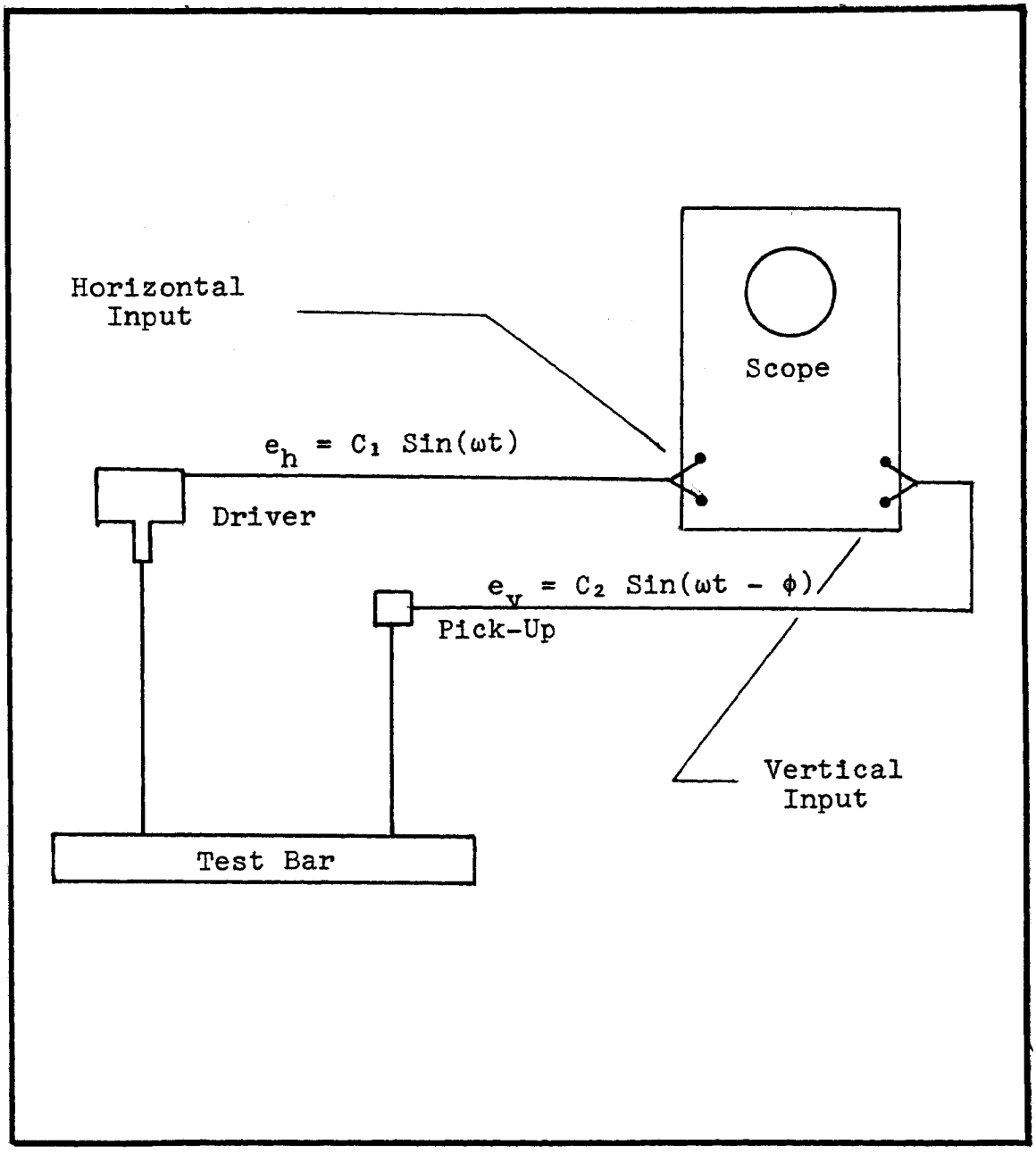

Figure 2. Frequency-phase set-up.

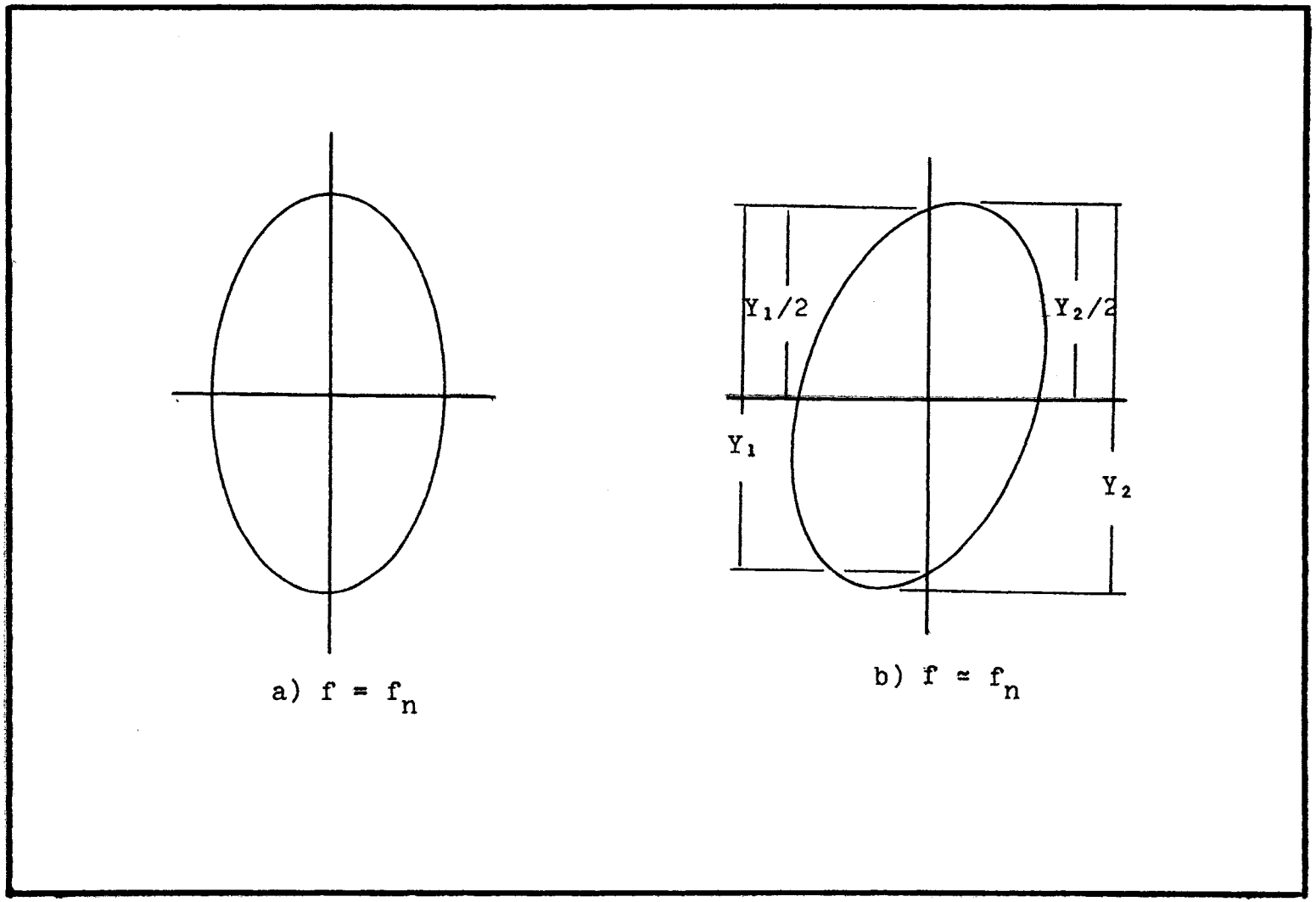

Figure 3. Lissajous figure orientations.

$$\phi = \sin^{-1} Y_1/Y_2 .$$

The tan ϕ may be determined from equation 28 and the logarithmic decrement may be computed by use of:

$$L.D. = (f_n/f - f/f_n)\pi \tan \phi . \qquad (29)$$

The natural frequency, f_n, is first determined by adjusting the frequency of the oscillator until the Lissajous figure is vertical. The oscillator frequency is then changed to a frequency, f, so the ellipse is tilted; at this frequency, the distances Y_1 and Y_2 are measured. It has been found convenient to keep one distance, Y_1, constant for all measurements, thus only Y_2 must be measured. Because very accurate frequency determinations are necessary, the output of the oscillator is fed to an electronic counter.

F. Surface Decoration Techniques

A count was made of the number of cracks along the length of the long rods prior to strength testing. This was done by drawing a thin line the length of the bar and counting the cracks which intersected the line. Three counts were made for each rod. Viewing of the cracks was facilitated by immersing the bars in carfusin dye. After the dye was dry, the excess was removed from the surface with acetone. The dye penetrated the samples at crack interfaces, thus leaving a distinct pattern on the surface.

Inasmuch as the dye penetrated the depth of the

cracks, it was also possible to obtain a measure of crack penetration as a function of thermal shock temperature difference. This was done by cutting sections out of shocked bars. Crack depths were then measured with dividers and a rule divided into 0.02 inch increments.

G. Determination of Heat Transfer Coefficient

It was necessary to know the surface heat transfer coefficient in order to fully specify the conditions under which the thermal shock is incurred. The surface heat transfer coefficient is a function of surface geometry, fluid characteristics, and the temperature difference. A rod of Armco iron six inches long by one inch in diameter was chosen to determine this parameter. Armco iron was chosen since the properties of this material are well documented[33,34].

A chromel-alumel thermocouple was embedded in the iron along the axis to a depth of three inches. This thermocouple was attached to a Houston Instrument Company x-y recorder having a range of time sweeps in the x direction from 0.05 inches per second to two inches per second. The iron rod was heated to preselected temperatures between 150°C and 500°C in the Hitec heat transfer salt. After a soak of one-half hour, to insure equilibrium temperature, the bar was plunged into a bath of ice water. The temperature decreases as a function of time were plotted automatically on the x-y recorder. These curves are presented in Appendix C.

In order to calculate the heat transfer coefficient, the curves obtained by this method were converted to dimensionless temperature, and were compared with theoretical curves by Heisler[35]. The coefficient (h) was found to be fairly constant over the range of interest; the value determined was 0.171 Cal/°C/cm^2/sec. This value should apply to other materials of the present geometry which are subjected to the conditions imposed in the present work.

IV. RESULTS

A. Strengths of Short Cylinders

Strengths and strength data dispersions as a function of thermal shock temperature difference are plotted in Figures 4 and 5 respectively. This data is also given in Table I. The number of specimens tested at each temperature difference is also given in Table I. No detectable strength deterioration was observed after a 150°C shock; however, a 175°C shock temperature difference (ΔT) resulted in a significant strength loss. Larger shock ΔTs resulted in still greater strength decreases. Two sets of data are given here: the full circles represent those samples which have received both a heating and cooling shock. Prior to strength testing, all cylinders were visibly inspected for cracks. No decoration techniques were used as the cracks were readily visible. Specimens shocked at 150°C ΔT showed no cracks while visible cracks were seen in 90% of all specimens shocked at 175°C. Individual cylinders having no visible cracks exhibited strengths equal to or greater than the mean strengths of the control groups.

Strength dispersions of the control samples and those samples shocked at 150°C ΔT showed no differences. Samples shocked at 175°C, the temperature difference where strengths first decreased, showed an appreciable increase in dispersion. With increasing shock ΔTs, however, the standard deviations decreased as seen. This behavior was

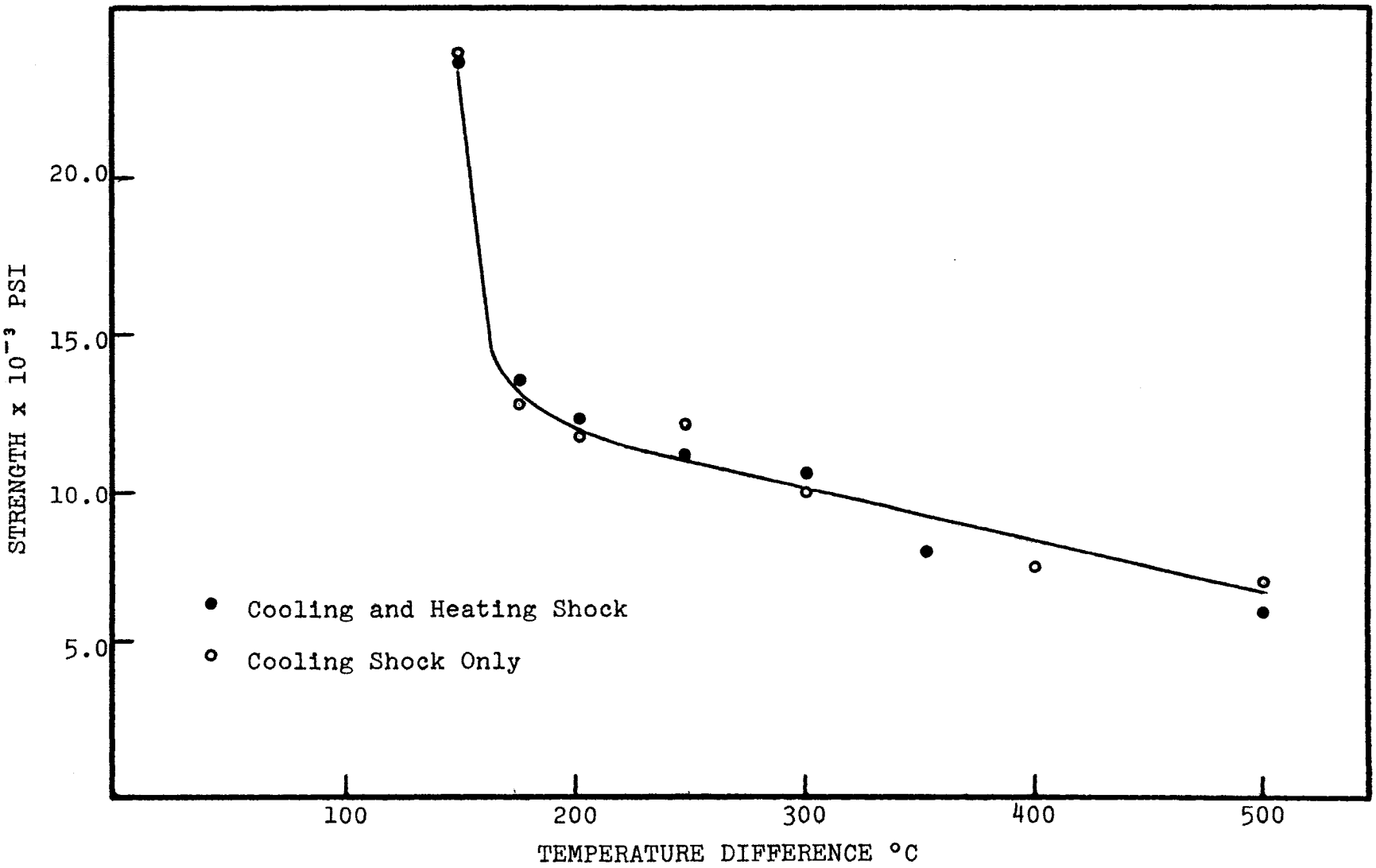

Figure 4. Strengths of short cylinders as a function of temperature difference.

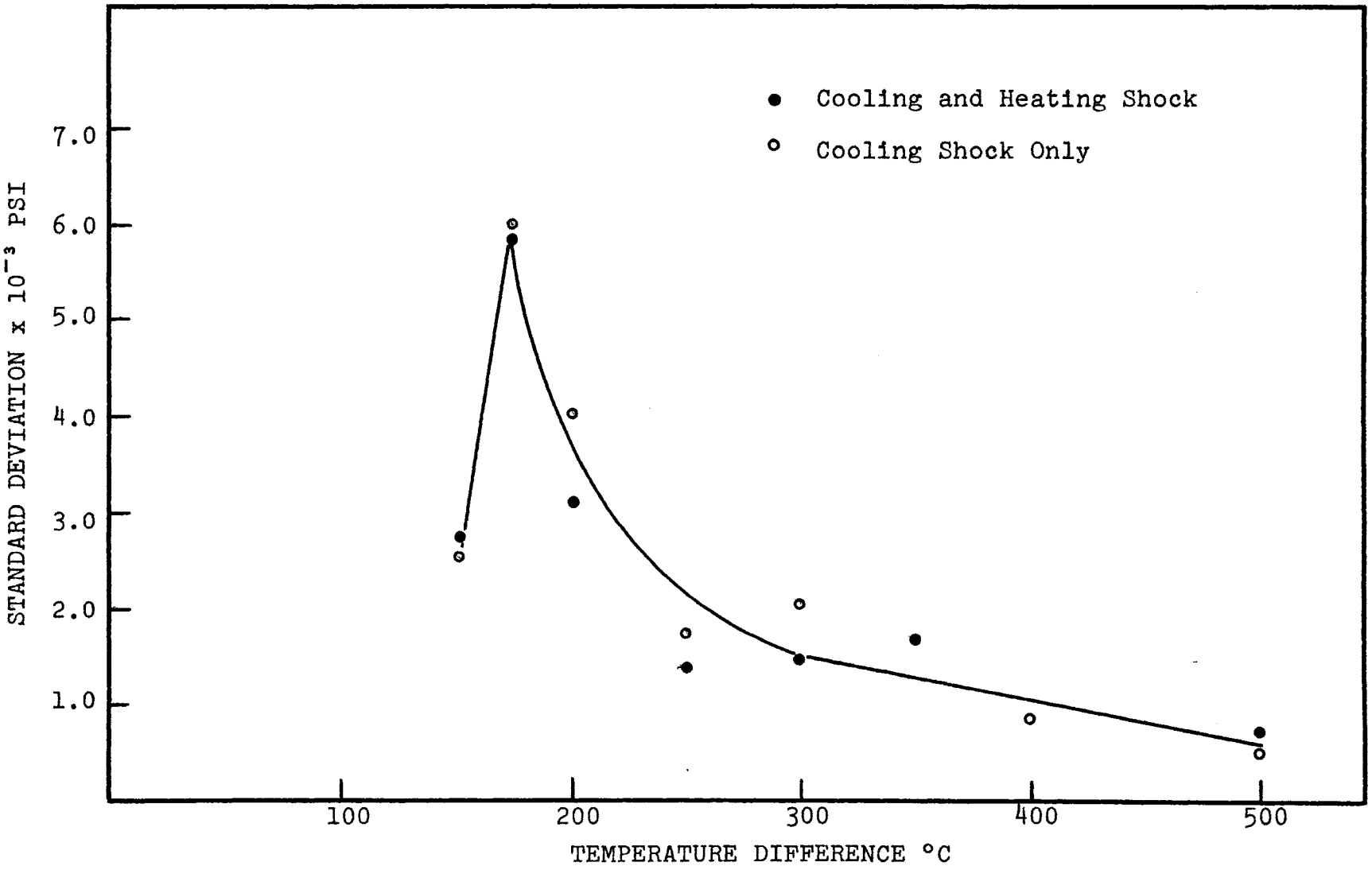

Figure 5. Strength data dispersions of short cylinders.

TABLE I

Strength Data on Short Cylinders

Group A — Heating and Cooling Shock Treatment				Group B — Cooling Shock Treatment Only			
Temperature Difference (°C)	Number Tested	Strength (Psi)	S. D. (Psi)	Temperature Difference (°C)	Number Tested	Strength (Psi)	S. D. (Psi)
Control Group	5	20,248	2,220	Control Group	5	22,700	2,160
150°C	10	23,340	2,680	150°C	5	23,700	2,430
175°C (Damaged)	8	13,340	5,920	175°C (Damaged)	5	11,930	5,940
175°C (Total)	10	14,366	5,320	175°C (Total)	5	11,930	5,940
200°C	8	11,630	3,080	200°C	4	12,052	3,400
250°C	5	10,370	1,340	250°C	5	11,158	1,510
300°C	5	9,840	1,370	300°C	5	9,166	2,010
350°C	5	7,538	1,530	400°C	5	7,058	526
500°C	4	4,670	833	500°C	5	5,980	529

characteristic of both sample sets.

A study was conducted to determine the effects of repeated cycling on the strengths of the short cylinders. Figure 6 gives plots of this strength data after one, two, and three cycles at shock ΔTs of 250°C, 300°C, and 350°C. The first cycle appeared to be the most damaging in all cases. Table II gives the strengths and strength-data dispersions. No trends were discerned from plots of standard deviations.

B. Strengths of Long Rods

In addition to the studies on the short cylinders, strength tests were performed on six-inch rods of the same diameter. Figure 7 shows the strength data developed for each shock temperature difference. All shocks on the long rods are cooling shocks. No strength decrease was noted after shocking at a ΔT of 150°C; however, a 175°C shock produced a significant strength loss. A slight trend to higher strength is noted at 200°C and 250°C, with the maximum at 250°C. From 250°C to 500°C, the strengths decrease in a linear fashion. This data is presented in Table III.

All test specimens were decorated with carfusin dye to facilitate obtaining relative crack densities and crack depths. To determine whether this dye had an effect on the strength, a sample of undecorated bars, shocked at 250°C, was tested. The mean strength of this sample is shown as a dark circle in Figure 7. No significant

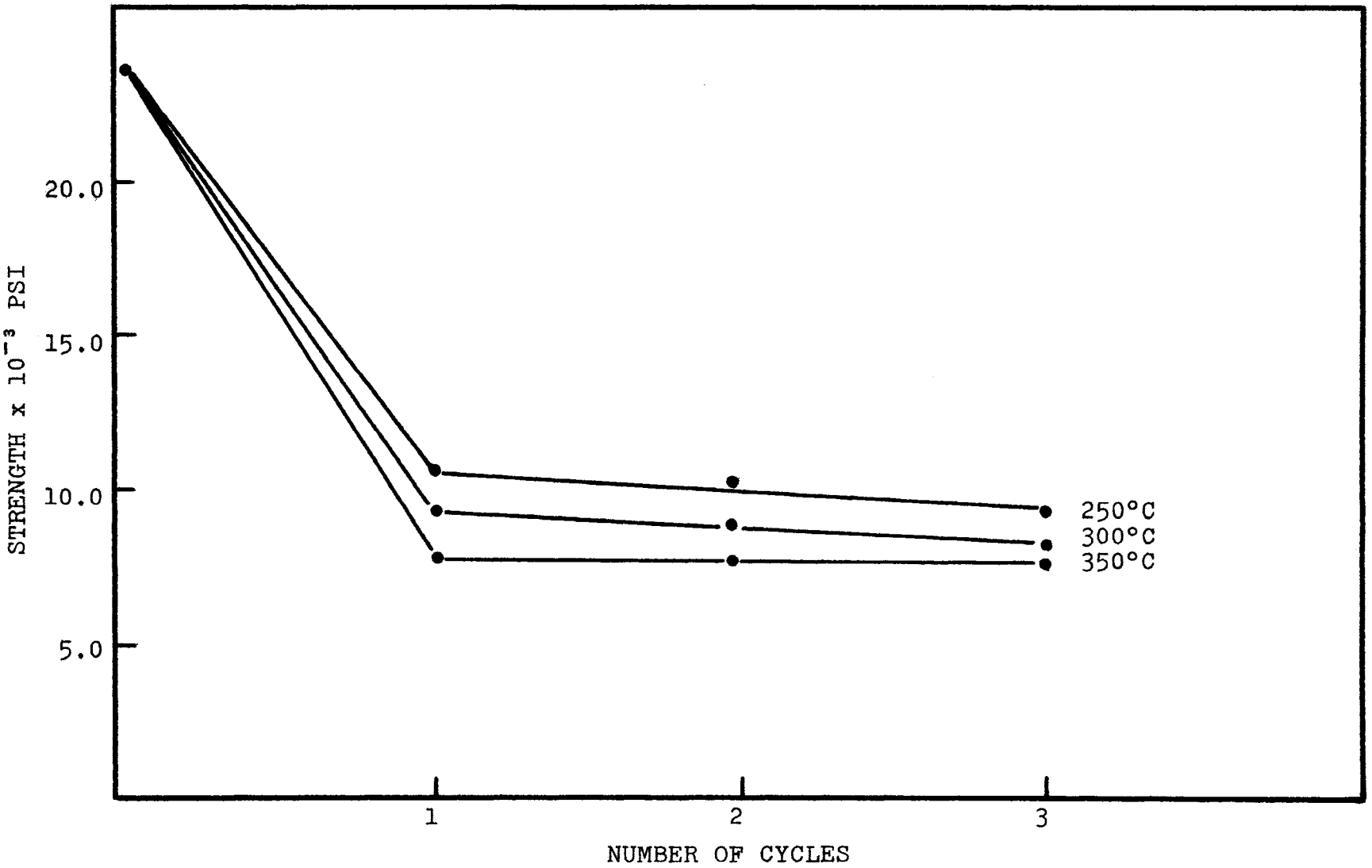

Figure 6. Strength decreases in short cylinders as a function of thermal shock cycles.

TABLE II

Strengths of Short Cylinders after Cycling

Number of Cycles	Temperature Difference (°C)	Number Tested	Strength (Psi)	S.D. (Psi)
-	Control Group	5	20,250	2,220
1	250°C	5	10,370	1,340
2	250°C	4	10,230	1,470
3	250°C	5	9,850	2,300
1	300°C	5	9,840	1,370
2	300°C	5	9,322	2,430
3	300°C	5	7,840	1,060
1	350°C	5	7,540	1,530
2	350°C	5	7,460	1,570
3	350°C	5	7,380	1,070

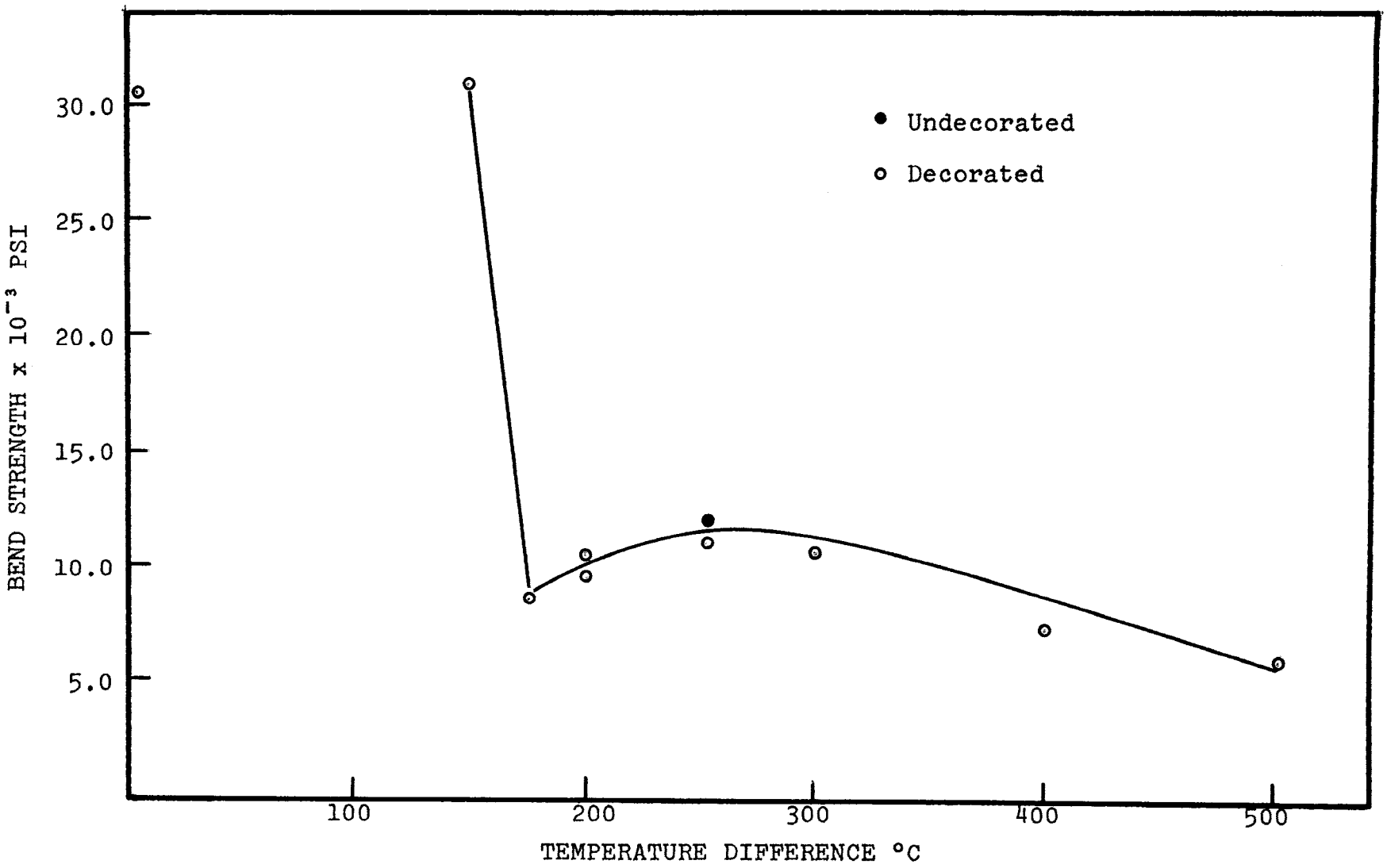

Figure 7. Strengths of long rods as a function of temperature difference.

TABLE III

Strength Data on Long Rods

Temperature Difference (°C)	Number Tested	Strength (Psi)	S. D. (Psi)
Control Group	5	30,923	2,310
150	5	31,200	1,065
175 (Damaged)	4	7,815	3,400
175 (Total)	5	12,770	5,100
200 (Sample A)	5	8,910	523
200 (Sample B)	5	8,386	800
250 (Undecorated)*	5	9,898	1,684
250	5	9,408	795
300	5	8,947	614
400	5	7,290	985
500	4	6,460	1,070

* With the exception of one sample (shocked at 250°C ΔT) all samples were decorated with carfusin dye.

difference was detected between the decorated and undecorated samples shocked at the 250°C level. Thus, this dye is not felt to affect bend strengths.

Figure 8 and Table III show the strength data dispersions of the long rods as a function of temperature difference. The standard deviation of the control group is higher than that of the sample shocked at 150°C ΔT. The sample shocked at 175°C ΔT exhibits a much higher dispersion as seen from the figure. Samples shocked from 200°C to 500°C are characterized by low dispersions.

C. Elastic and Anelastic Properties of Long Rods

Modulus of elasticity data and logarithmic decrement data are given in Table IV. Figure 9 shows the behavior of Young's modulus with shock temperature difference, and Figure 10 gives the logarithmic decrement as a function of ΔT. It can be seen that with increasing shock severity, Young's modulus decreases and the internal friction increases. No change is seen in either of these properties after shocking at 150°C ΔT. Shocking at 175°C produces a decrease in Young's modulus and an increase in the logarithmic decrement.

D. Crack Characteristics of Long Rods

1. Crack Densities

The densities of cracks increase significantly from 175°C ΔT to 500°C ΔT. This data is given in Table V and shown in Figure 11. It must be emphasized that this does not represent the actual number of cracks, but is simply

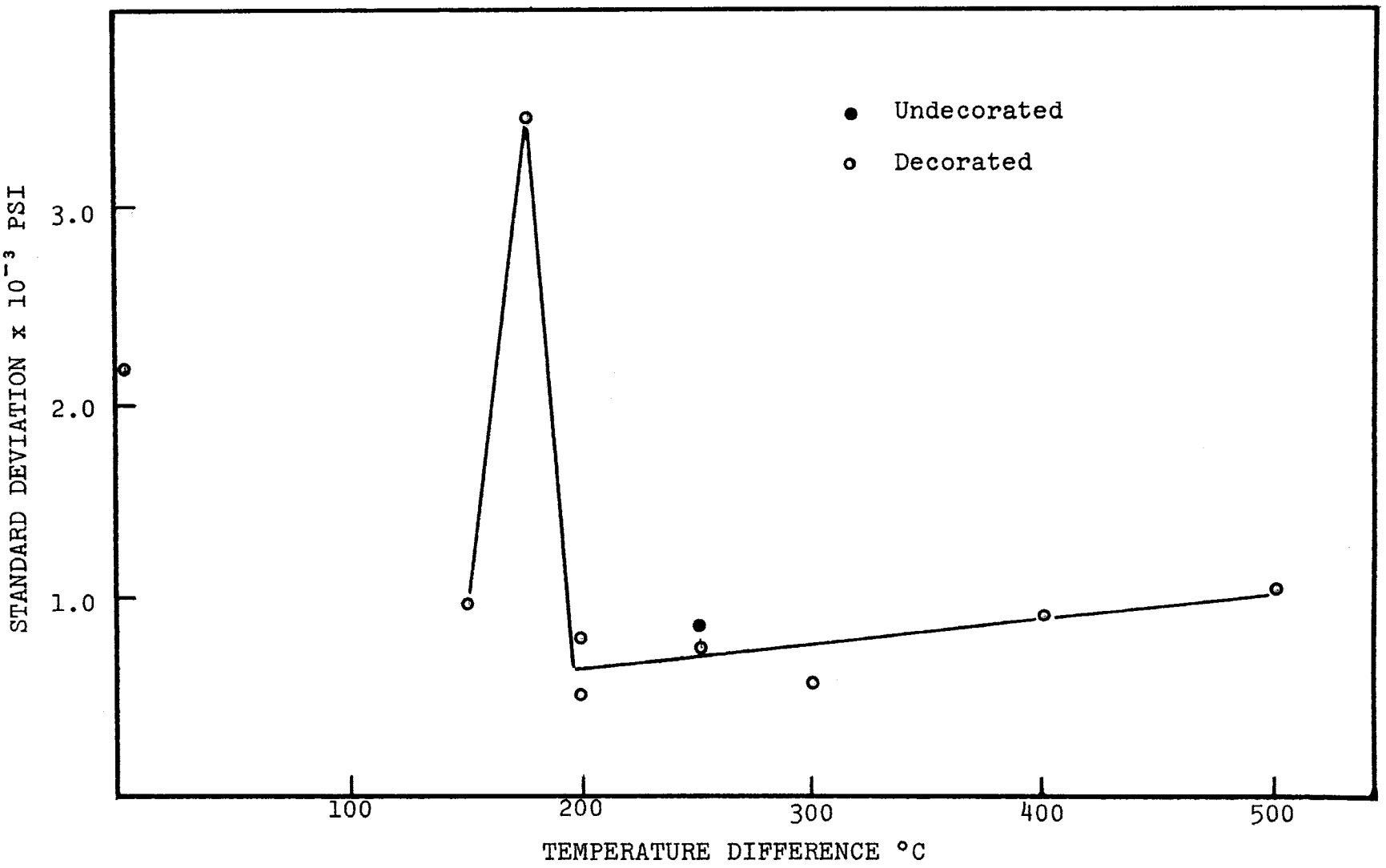

Figure 8. Strength data dispersions of long rods.

TABLE IV

Modulus of Elasticity and Logarithmic Decrement

E-Modulus

Temperature Difference (°C)	Number Tested	E x 10^{-6} (Psi)	S x 10^{-6} (Psi)	% Change
Control Group	80	53.9	0.455	-
150°C	5	53.8	0.284	0
175°C	5	53.5	0.731	0.74
200°C	6	53.0	1.132	1.34
250°C	6	50.7	0.786	5.31
300°C	6	49.3	0.638	8.13
400°C	5	45.9	0.515	14.71
500°C	5	41.5	0.661	22.69

Logarithmic Decrement

Temperature Difference (°C)	Number Tested	α x 10^{-4}	S
Control Group	80	2.57	-
150°C	5	2.94	1.24
175°C	5	7.44	3.40
200°C	6	11.90	0.96
250°C	6	82.30	20.40
300°C	6	119.00	40.00
400°C	5	104.00	28.00
500°C	5	183.00	19.00

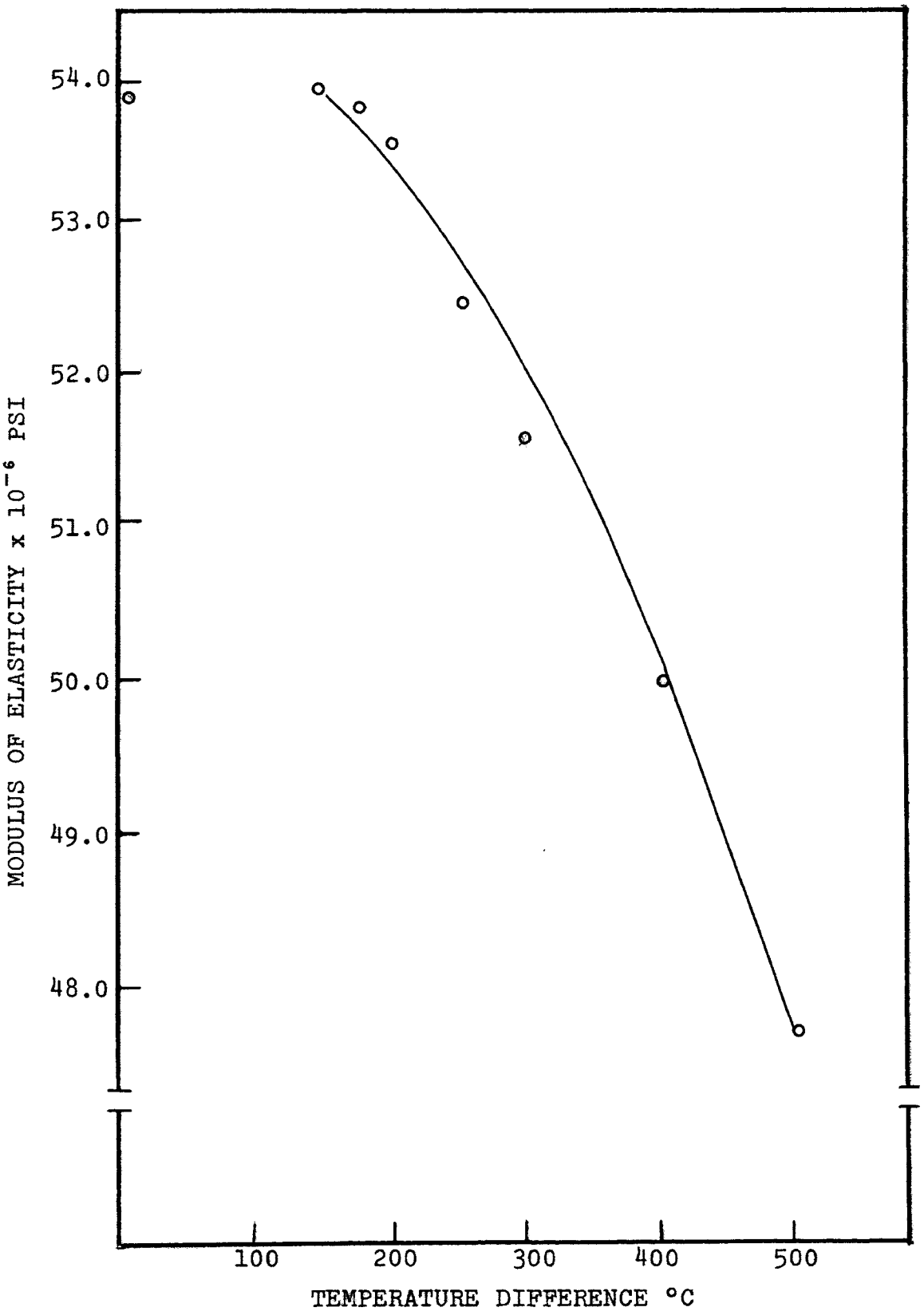

Figure 9. Elastic modulus as a function of shock temperature difference.

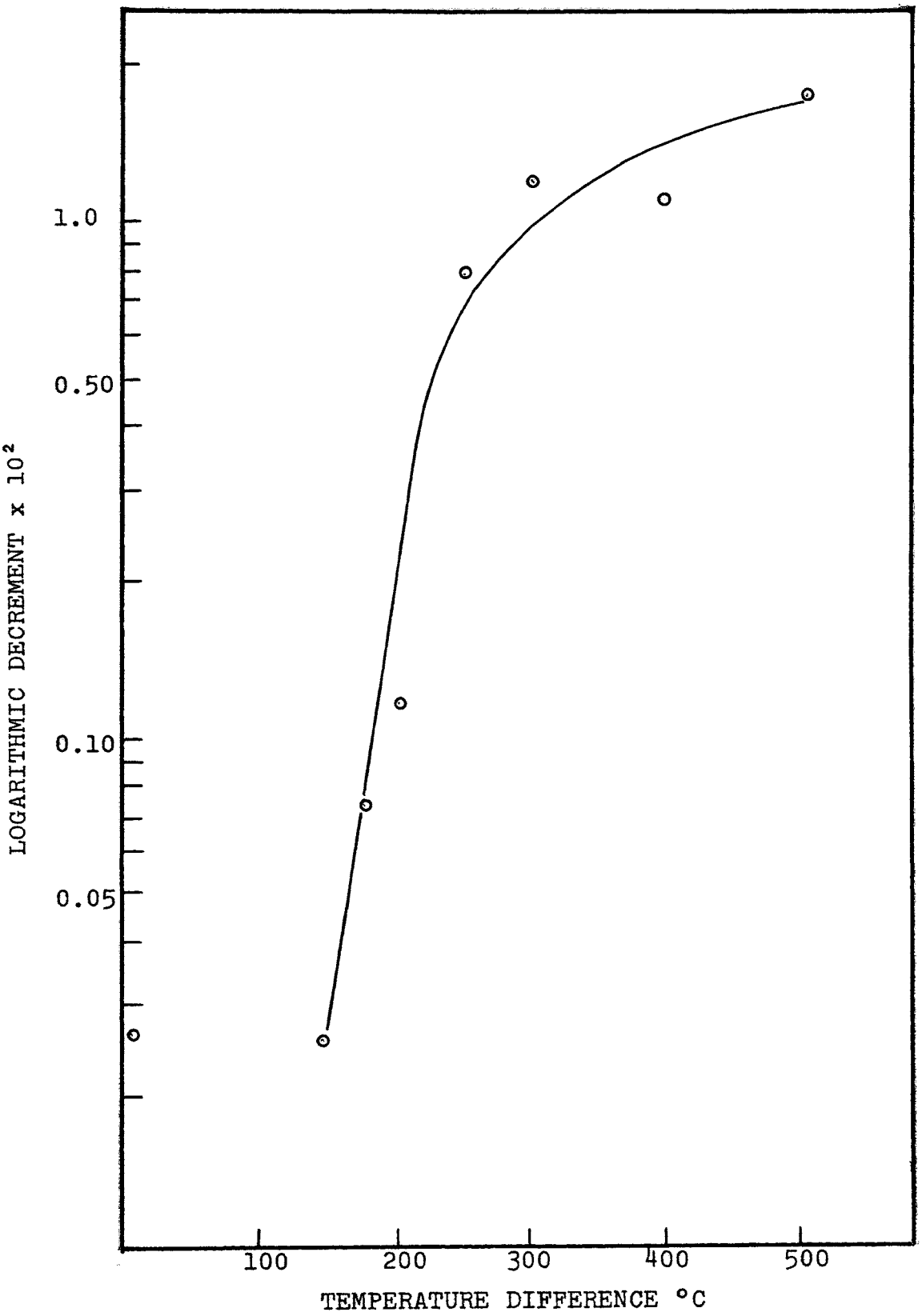

Figure 10. Internal friction as a function of shock temperature difference.

TABLE V

Crack Densities in Long Rods

Relative Crack Densities

Temperature Difference °C	Number of Bars Observed	Density Number of Cracks Crossing a 1" Line
150°C	-	-
175°C	3	1.0
200°C	3	6.5
200°C	3	7.0
250°C	4	14.0
250°C	3	11.0
300°C	4	14.0
400°C	3	17.5
500°C	3	21.0

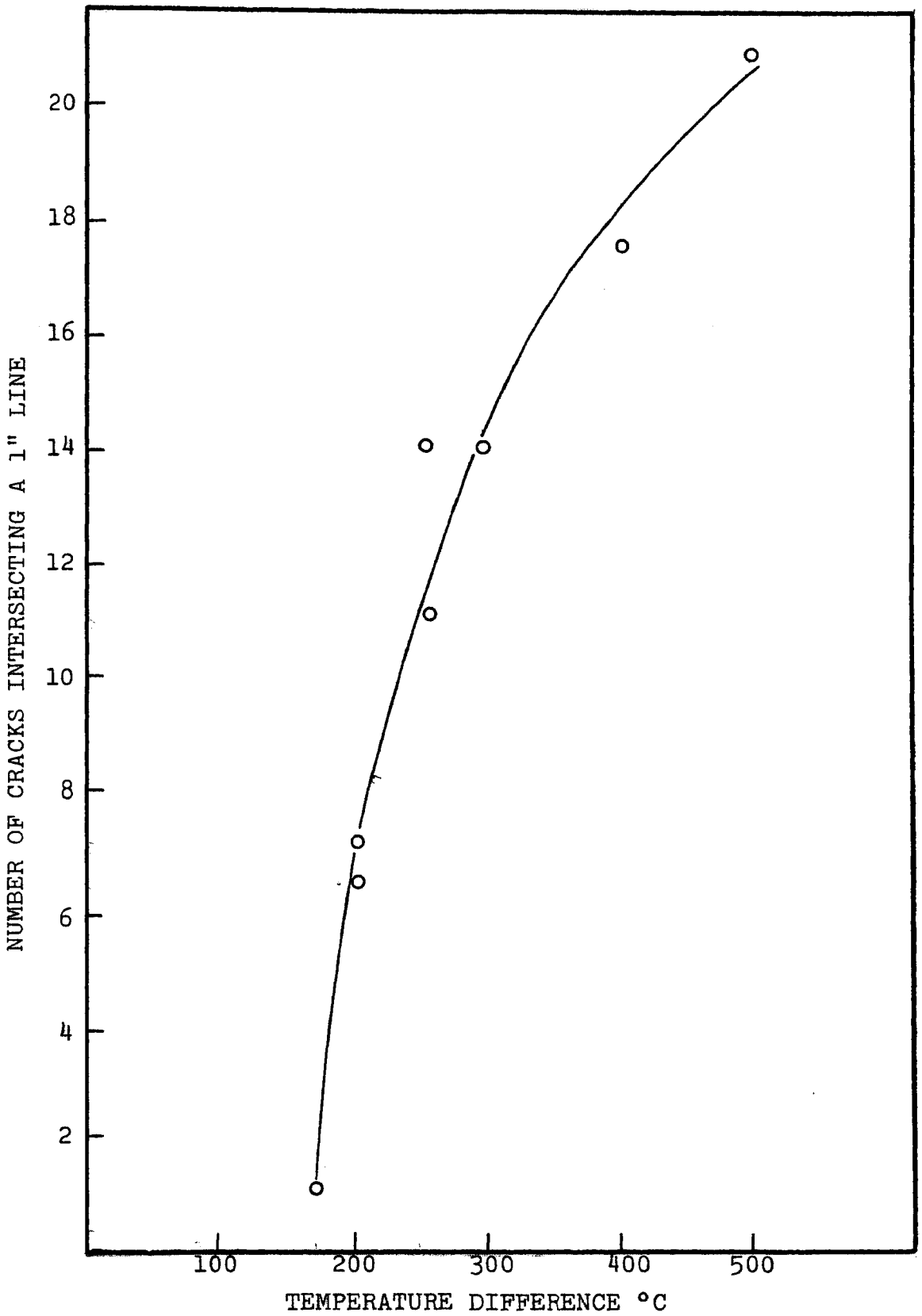

Figure 11. Crack densities as a function of thermal shock level.

a relative measure of crack density increases.

2. Crack Depths

Figure 12 shows plots of the tangential and axial crack depths as a function of shock temperature difference. These data are presented in Table VI. The depths are seen to decrease at 200°C and 250°C. An increasing trend is seen from 250°C ΔT to 500°C ΔT.

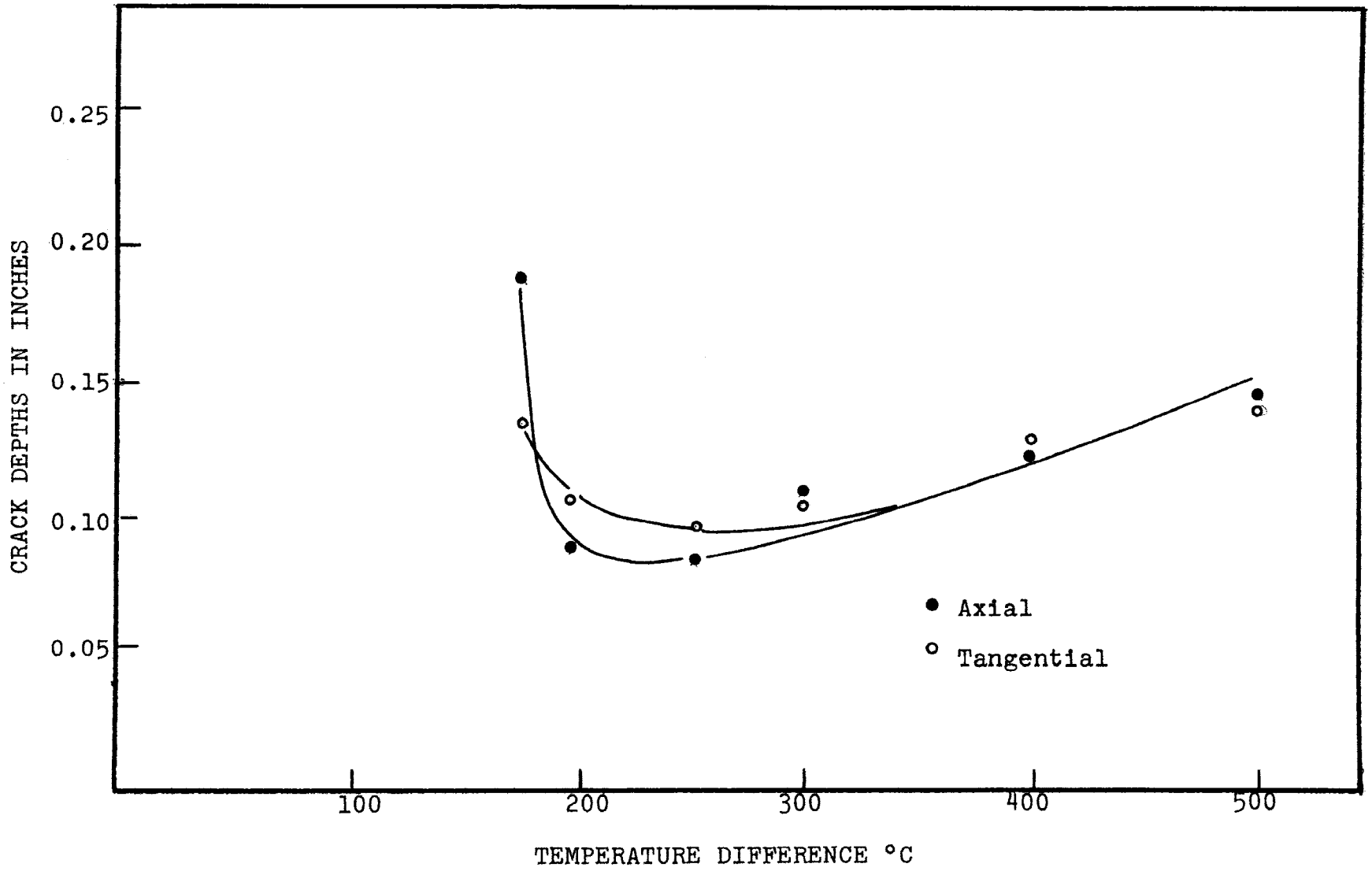

Figure 12. Crack depths resulting from thermal shock.

TABLE VI

Crack Depths in Long Rods

Average Crack Depths

Temperature Difference °C	Number of Bars Observed	Axial Crack Depths	S.D.	Tangential Crack Depths	S.D.
150°C	-	-	-	-	-
175°C	3	.20"	.04"	.14"	.04"
200°C	3	.11	.01	.09	.02
250°C	3	.10	.01	.08	.01
300°C	3	.11	.01	.11	.01
400°C	3	.13	.01	.13	.01
500°C	3	.15	.01	.15	.01

V. DISCUSSION

A. General Analysis of Measurements on Short Cylinders

It is recalled that two complete sets of short cylinders were shocked. One set received both heating and cooling shocks; whereas, the second set received cooling shocks only. Agreement between the two sets is felt to be quite good, especially in view of the small sample sizes. Statistically, no significant differences were found between corresponding data points except at the 500°C shock level. Since one sample set received both heating and cooling shocks, while the other set received only cooling shocks, the differences at the 500°C level are attributed to variations in the shock programs. It is felt that damage on heat-up shocks does not occur until a temperature difference of 400°C is attained.

The curve in Figure 4 indicates that incipient damage occurs between 150°C and 175°C. Although no data was taken in this interval, this region would lend itself well to a distribution plot of damage frequency versus ΔT. At 160°C ΔT, for example, 20% of the cylinders might be damaged. This procedure is common in thermal shock testing[27]. The present data indicates that, even at 175°C ΔT, damage frequency is less than 100%.

The strength decrease resulting from a 175°C shock is large in comparison to strength losses from more severe shocks. If a trend of this nature were to continue, zero

strength or complete failure would be observed at a 200°C shock level. A least squares determination for the data from 175°C to 500°C gave the following relation:

$$\sigma = -17.2\ \Delta T + 14{,}700. \qquad (30)$$

This relation predicts zero strength at a ΔT of 850°C.

The strength data dispersions proved to be quite interesting and somewhat unique. At low ΔT values where damage was first observed, the standard deviation increased appreciably. As more severe shock levels were imposed, dispersions decreased, until at 500°C ΔT, they were well below those of undamaged samples. Similar behavior has been observed by Daniels[36] and others[37], and more will be said about this phenomenon later.

The short cylinders were subjected to repeated shocks of one, two, and three cycles at three temperature differences. The strength data is shown in Figure 6. In each case, all damage is incurred on the first cycle. Possibly a test of this nature should be carried out over a larger number of cycles such as twenty-five or even fifty. Lack of material made such an experiment unfeasible in the present case. It is probable that damage resulting from the first shock acts to relieve stresses arising on succeeding shocks and further damage would be lessened.

B. General Analysis of Measurements on Long Rods

As in the case of the short cylinders, the long rods exhibit initial damage between 150°C and 175°C. Within

this range, the percent of damaged rods for a given ΔT can be plotted on a distribution curve. In the case of the long rods, 80% of the specimens showed damage after the 175°C shock.

It is seen from Figure 7 that the strength losses associated with the 175°C shock are followed by slight strength increases at 200°C and 250°C. This behavior is not unexpected in view of the trends taken by the crack depths (Figure 12). That is, these strength values reflect the trends of the crack depths. A least squares plot of the data shows behavior following the relation:

$$\sigma = -12.2\ \Delta T + 14{,}900. \qquad (31)$$

This equation predicts complete failure, i.e. zero strength at $\Delta T = 1215°C$. Since data was only taken to shock ΔTs of 500°C, this value of 1215°C represents better than a 700°C extrapolation, and must be considered questionable.

The standard deviation of the long rods exhibits a behavior very similar to that shown by the short cylinders. With the first strength decreases, the standard deviation increases, and with subsequent more severe shock levels, appreciable decreases are noted.

It is seen from Table VI that crack depth dispersions are largest at the 175°C shock level. This greater variance in crack depths could contribute to the larger variance in strengths.

In his work on a triaxial porcelain, Daniels[36] induced artificial flaws along the lengths of the porcelain bars. These flaws were oriented perpendicular to the direction of maximum stress. He detected no increase in dispersion, but instead saw an immediate decrease when flaws were induced. It has been shown in the present work, that early damage is characterized by a dispersion increase. As stated above, variances in crack depths could be responsible; however, a second possible explanation for the differences between Daniels' observations and the present observations lies in flaw orientation. When a bar is stressed in the present investigation, failure occurs at a point previously weakened by thermal shock damage. A flaw oriented perpendicular to the direction of applied stress is more damaging than a flaw oriented parallel to the applied stress. Deviations of flaws from these two extremes would affect the failure stress in accordance with orientation. At 175°C ΔT, the crack densities are low, and the cracks are randomly oriented with respect to the applied stress. This is a major deviation from the conditions in Daniels' work. As the ΔT levels increase, a network of closely spaced cracks develops. When a stress sufficient to cause failure is applied to the bars, fracture occurs at a flaw, composed of several cracks within the crack network, which is effectively oriented perpendicular to the applied stress. Thus, conditions similar to those of Daniels' are

approached.

The logarithmic decrement data and modulus of elasticity data serve as supplements to the strength data. It was hoped that the logarithmic decrement might be more sensitive than the strength determinations in detecting early damage. However, the first changes in logarithmic decrement were observed after a 175°C shock. Thus one more piece of data exists to verify the observation that no damage is initiated after a shock of 150°C ΔT.

A definite advantage in using non-destructive tests of this nature lies in the testing before shocking and after shocking. Any doubt concerning damage can be removed by viewing the "before" and "after" data on each bar.

It is seen that neither the logarithmic decrement nor the elastic modulus gives an indication of the crack depth decrease at 200°C and 250°C as indicated by the strength measurements. These measurements are taken using cyclic stresses near 4,000 cps, and they appear to give an indication of the overall damage to the material.

Inspection of the data suggests a possible inverse relation between the crack densities and Young's modulus. It would be expected that flaws oriented perpendicular or nearly perpendicular to the length would have the greatest effect on the modulus values. These are the flaws used to get an indication of densities; and relate to the apparent inverse relationship.

C. Comparison of Strength Measurements of Rods and Cylinders

The strength data of both the long rods and short cylinders suggest that there is little difference in the initial fracture ΔT for the two geometries and tests. Apparently the ends of the short cylinders have little effect with respect to heat flow, and the radius is the governing dimension. Also, with both geometries, the initial strength decreases are quite severe and more intense shocking does not yield equivalent decreases.

A proposed model of flaw orientation was given to explain the behavior of strength dispersions of the long bars. The trends in strength data dispersions of the short cylinders are quite similar, and it is probable that the same model would explain this behavior.

The strength increases seen for the long rods at 200°C and 250°C ΔT are not noted for the short cylinders. This probably reflects the method of testing.

D. Predictions of Damage in Terms of Crack Depths

Cooling thermal shocks seldom lead to catastrophic fracture, at least for ΔTs sufficient only to initiate cracks; thus, it would be of benefit if one could predict the degree of damage caused by cooling shocks. A criteria for describing this degree of damage is the depth to which cracks penetrate from the surface. Data on crack depths were presented previously; however, no discussion has yet been undertaken.

Lachenbruch[38,39] appears to have presented the only work available for predicting crack depths under conditions

approaching those imposed by cooling shocks. He proposed the following equation for calculating crack depths in a semi-infinite medium exposed to surface contraction cracks (see Appendix A for a list of symbols):

$$\Sigma A_i \sqrt{b}\ \Gamma(d_i/b) - 0.68\rho g b^{3/2} = \left[\frac{\gamma E}{(1-\mu^2)\pi}\right]^{1/2}, \qquad (32)$$

where A_i = stress acting on an increment of thickness d_i,

$\Gamma(d_i/b)$ = the normalized stress intensity factor,

b = crack depth, and

g = gravimetric constant.

For the present purposes, the term:

$$0.68\rho g b^{3/2},$$

representing the contribution of gravitational compression, can be neglected. Equation 32 may, therefore, be written as:

$$\Sigma A_i \Gamma(d_i/b) = \left[\frac{\gamma E}{(1-\mu^2)\pi}\right]^{1/2}. \qquad (33)$$

Values of $\Gamma(d_i/b)$, a normalized crack-edge stress intensity factor, are given in Table VII. Figure 13 shows that for d/b ratios less than 0.6, $\Gamma(d_i/b)$ is equal to $0.8\ d_i/\sqrt{b}$ Thus, equation 33 may be written as:

$$\Sigma A_i\ 0.8\ d_i/\sqrt{b} = \left[\frac{\gamma E}{(1-\mu^2)\pi}\right]^{1/2}. \qquad (34)$$

A crack will continue to propagate as long as the left hand

TABLE VII

Normalized Stress Edge Intensity Factors

d/b	0.05	0.1	0.2	0.3	0.5	0.75	1.0
Γ(d/b)	0.04	0.08	0.16	0.24	0.41	0.64	1.1

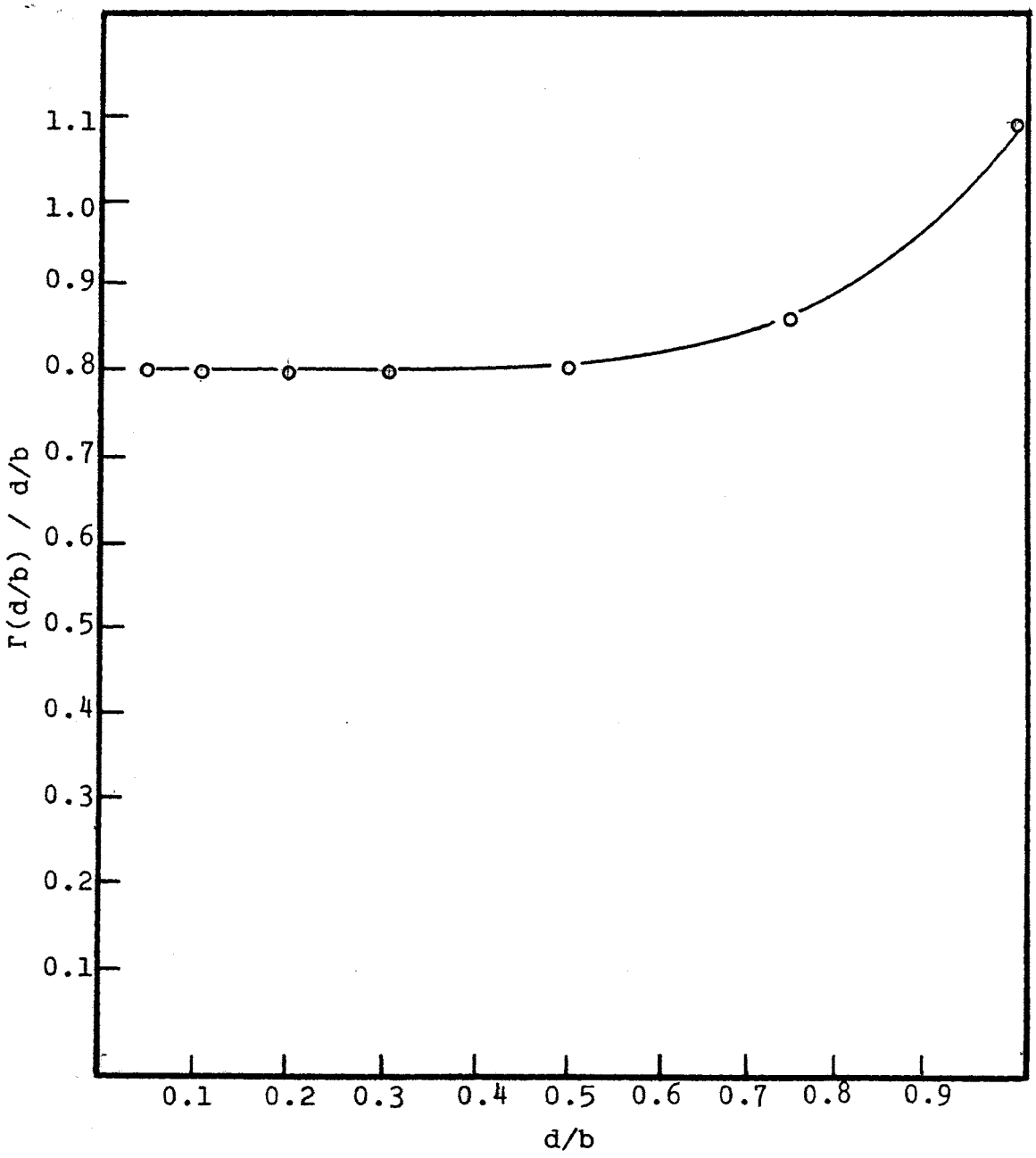

Figure 13. Relationship between Γ(d/b) and d/b.

side of equation 34 exceeds the right hand side. Close to the surface, tensile stresses will contribute to crack propagation; however, as the crack passes from the region of tension into the compressive region, the compressive stresses will act to eventually arrest the crack.

The use of equation 34 in predicting crack depths requires a knowledge of the thermal stresses set up in the test specimens. Jaeger's equations (Appendix B) were employed to determine these stresses. The material properties necessary for the calculations of both thermal stresses and crack depths are given in Appendix D. The stress distribution in the tangential direction for a ΔT of 175°C is shown in Figure 14. In order to apply equation 34, this distribution was approximated with discrete stress steps of thickness "d" as shown. The results of calculations using the known material properties and equation 34 are shown in Figure 15. The experimental crack depths are also shown in this figure.

Good agreement exists between the observed and predicted crack depths at 175°C ΔT; however, with increasing ΔTs, the experimental data deviates from that predicted by equation 34. Lachenbruch has stated that the model is good as long as there are no crack interactions. It appears, however, that crack interactions do occur at higher shock ΔTs. These interactions occur with increases in crack densities. Figure 11 shows that the relative crack densities are low at 175°C ΔT, but increase appreciably at

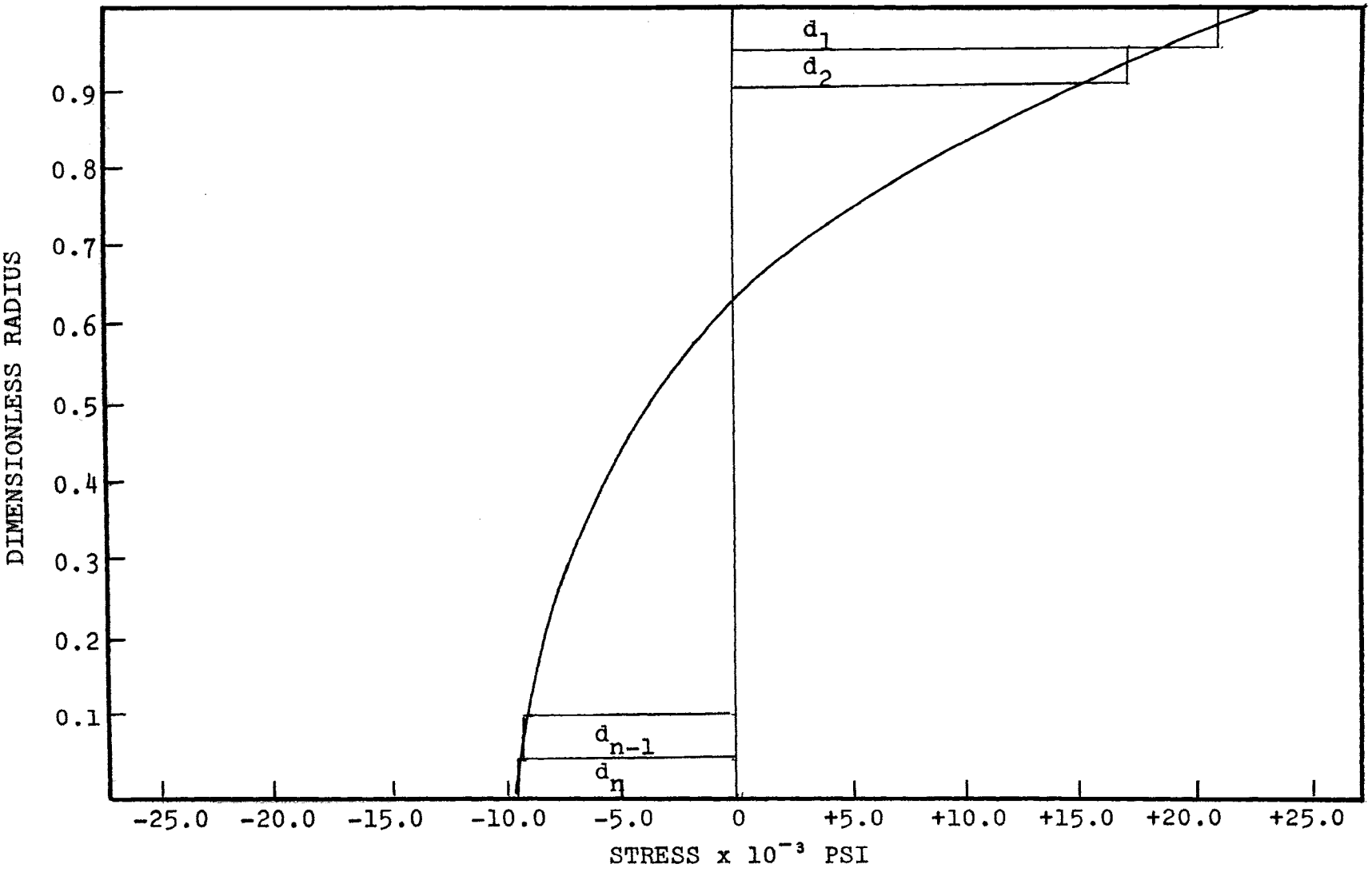

Figure 14. Stress distribution in tangential direction at 175°C.

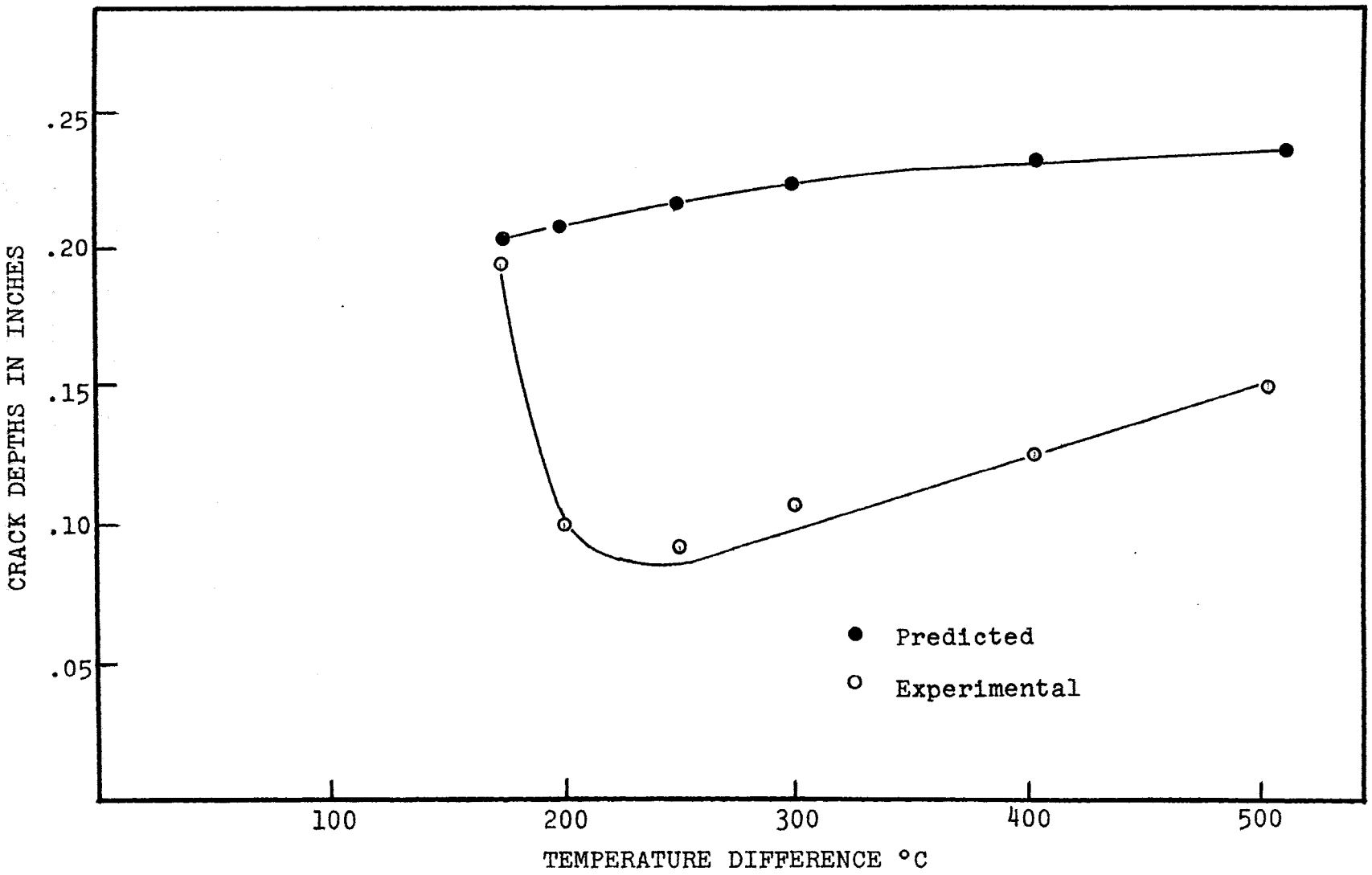

Figure 15. Predicted and observed crack depths.

higher ΔT levels. As crack densities increase, the elastic strain energy at fracture must be divided among a larger number of cracks. This explains the behavior seen at 200°C and 250°C ΔT. In this interval, the crack density increases significantly, but the elastic strain energy is not enough greater to drive the cracks deeper than those at 175°C ΔT. As the ΔT levels increase, the elastic strain energy increases at a rate sufficient to drive the increasing number of cracks deeper; thus, the increasing crack depth trend above the 250°C ΔT level.

It now becomes necessary to offer an explanation as to why crack densities increase with increasing ΔT levels. There appear to be three mechanisms which could account for this behavior. The first is simply the distribution of flaws on the surface. At stress levels just sufficient to cause fracture, the weakest flaw is probably responsible. At higher ΔTs and thus higher stress levels, cracks can be initiated from flaws stronger than the weakest flaw.

A second mechanism responsible for large crack densities is crack branching. As the stress state at the surface rises, the velocity of the crack propagating on the surface increases, and as a critical velocity is reached, crack branching may be promoted. Glenny[29] supports the above statement saying that cracks originating from the cooling shock are produced at the surface by axial tensile or circumferential tensile stresses or a combination of both. The crack lies in the region of

maximum stress and as a result branches quite readily.

A third mechanism leading to high crack densities is related to the anisotropic nature of Al_2O_3. If one considers two alumina crystals lying side by side on the surface, and if one considers those crystals to be oriented in different crystallographic directions, then severe shear stresses may be set up at the grain boundary as a result of differing thermal expansion coefficients. Johnston[17] has stated that such stresses would be difficult to calculate accurately, but an estimate suggests that they are extremely high. Johnston also suggests that it is quite possible that shear stresses at grain boundaries are in fact the initial cause of crack nucleation.

The considerations presented using Lachenbruch's work are gross simplifications. It is seen, however, that agreement is good at the low shock level. At these levels, application of such an explanation is reasonable in view of the small crack densities. It must be emphasized that here we are dealing with a finite body; thus, the stress states are probably quite different from those of an infinite body. It is also noted that once a crack is initiated and travels to any depth, the stress distribution in the material is changed drastically. Another fact to be considered is that we are dealing with transient stress states.

E. Agreement Between Theory and Experiment for Crack Initiation

Although the purpose of this work was not necessarily to determine the ΔT at which fracture occurs, all information was available to compute this value. It was stated earlier that experimentally, the initial fracture ΔT occurred between 150°C ΔT and 175°C ΔT. Using the known properties of the material (Appendix D), a value of 184°C was determined with Jaeger's[8] equations. This agreement is considered quite good.

Some discussion is in order regarding the temperature level at which material properties were selected. The thermal stress equations consider the thermal conductivity and the surface heat transfer coefficient to be constant over the entire temperature range. Figure 18 shows that this is not true for the thermal conductivity. If we were considering shocking on heating, considerable error could be introduced in the prediction of ΔT_{max} since thermal conductivity at temperatures near room temperature is so strongly temperature dependent. For the present case, that is, thermal shock on cooling, the selection of the correct value of thermal conductivity is less strongly dependent on temperature. The error in the selection of a thermal conductivity value is probably less than 10%.

Strength of Al_2O_3 is only slightly affected by temperature. Nevertheless, fracture is initiated at the surface, and thus the strength value should be selected at a lower temperature. The same consideration applies to the elastic modulus.

The thermal stress equations assume isotropic conditions. Aluminum oxide single crystals are anisotropic; however, a fine-grained, polycrystalline alumina such as that used in the present work is considered to be isotropic on a macroscopic scale. Therefore, use of the thermal stress equations is reasonable.

F. Discussion of Thermal Shock Techniques

The testing techniques used in this work are well suited to obtaining a quantitative indication of the degree of damage. Using this approach of measuring strength as a function of ΔT_s also shows that simply finding the determination of the initial ΔT to cause fracture does not always give all the necessary information. There is useful strength left in the bodies tested in this work even after a 500°C shock. The author has tested materials having less strength in their undamaged state. It must be emphasized that the application of the material is of prime importance when considering permissible damage. Some applications will tolerate no damage whatsoever. In other applications, damage is acceptable, to a limited extent. It now becomes a matter of deciding which is important: no damage or low damage. By determining the strength over a range of ΔT_s, one can bracket the ΔT at which damage is initiated. Thus, a test of this nature gives the experimenter two pieces of information:

1) the ΔT necessary to initiate fracture and

2) the degree of damage as a function of ΔT.

If it is desired to find only the initial ΔT to cause damage, the approach used in the present work proves to be redundant. There is little doubt that the material is undamaged after a 150°C shock. Thus, a number of the testing techniques can be eliminated. Bend testing or logarithmic decrement measurements could provide all the information needed.

VI. SUMMARY AND CONCLUSIONS

Thermal shock damage to Western Gold and Platinum Company 995 Al_2O_3 has been studied in the shock temperature difference range of 150°C to 500°C. Thermal shock conditions were imposed on preheated test specimens by quenching these specimens in ice water. Strength measurements and sonic analysis were the main quantitative tools used in the study. Early damage is characterized by large strength decreases and appreciable increases in strength data dispersion. Crack depths were found to be an effective criteria for degree of damage. Theoretical predictions of crack depths based on fracture criteria have proved to be in good agreement at low shock levels; crack interactions with increasing crack densities are the prime reason for deviations of observed crack depths from predicted crack depths. Increased crack densities can be explained by three factors: anisotropy, surface flaw distributions, and crack branching.

The following conclusions have been made from the work presented herein:

1. Under the conditions imposed in this study, Al_2O_3 exhibits no detectable damage after a 150°C shock. Useful strength is still present after shock treatments at 500°C.
2. Strength testing of thermally shocked material provides a good quantitative indication of the

degree of damage, and it provides a sensitive tool for determining the initial damage temperature difference.

3. Sonic analysis has shown itself to be of limited usefulness since it is less sensitive to crack depth behavior than the strength testing. Sonic analysis is sensitive to crack density increases, however.
4. Crack densities do not provide a measure of the degree of damage. High crack densities act as a deterrent to damage on cooling shocks.
5. Lachenbruch's equation is limited to low temperature shock treatments which result in low crack densities.

VII. RECOMMENDATIONS FOR FUTURE WORK

The following recommendations are made for future work:

1. A rigorous study of the effects of repeated thermal shocks is needed. Such a study would establish if damage increases after a large number of shock cycles.

2. An experimental program, similar to the present program, involving a large number of brittle materials should be initiated. The materials studied should include both isotropic and anisotropic materials. Such an investigation would be most useful in determining the effects of anisotropy on damage resulting from cooling thermal shocks.

3. In order to determine the degree of damage to a given material, it is necessary to know the effective surface energy. A program should be conducted to measure this property on a wide range of materials.

4. In addition to studies on single phase systems, it is recommended that work be initiated to investigate polyphase systems. Many ceramic bodies currently used are polyphase bodies, and better characterization of the effects of phase combinations on thermal shock resistance and damage resistance would be helpful.

BIBLIOGRAPHY

1 D. P. H. Hasselman, "Elastic Energy at Fracture and Surface Energy as Design Criteria for Thermal Shock", J. Am. Ceram. Soc., 46 (11) 535-540 (1963).

2 F. A. Hummel, "Ceramics for Thermal Shock Resistance", Ceramic Industry.

3 A. Winkelman and O. Schott, "Uber Thermische Widerstandscoefficienten verschiedener Glaser in ihrer Abbangigkeit van der chemischen Zus ammensefzung", Ann. Physik und Chem., 51, 730 (1894).

4 W. D. Kingery, "Factors Affecting Thermal Stress Resistance of Ceramic Materials", J. Am. Ceram. Soc., 38 (1) 3-15 (1955).

5 D. P. H. Hasselman, "Thermal Shock by Radiation Heating", J. Am. Ceram. Soc., 46 (5) 229-234 (1963).

6 D. P. H. Hasselman, "Theory of Thermal Shock Resistance of Semitransparent Ceramics Under Radiation Heating", J. Am. Ceram. Soc., 49 (2) 103-104 (1966).

7 D. P. H. Hasselman, "Approximate Theory of Thermal Stress Resistance of Brittle Ceramics Involving Creep", J. Am. Ceram. Soc., 50 (9) 454-457 (1967).

8 J. C. Jaeger, "On Thermal Stresses in Circular Cylinders", Philosophical Mag., 36 (257) 418-428 (1945).

9 M. J. Lighthill and F. J. Bradshaw, "Thermal Stresses in Turbine Blades", Philosophical Mag., 40, 770-780 (1949).

10 B. E. Gatewood, "Thermal Stresses in Long Cylindrical Bodies", Philosophical Mag., 32, 282-301 (1941).

11 F. J. Bradshaw, "Thermal Stresses in Non-Ductile High Temperature Materials", Tech. Note MET. 100, British RAE, Feb. 1949.

12 W. Buessem, "Ring Test and its Application to Thermal Shock Problems", O. A. R. Report, Wright-Patterson Air Force Base, Dayton, Ohio, 1950.

13 S. S. Manson, "Behavior of Materials Under Conditions of Thermal Stress", N. A. C. A. Tech. Note No. 2933, July 1953.

14 R. L. Coble and W. D. Kingery, "Effect of Porosity

on Thermal Stress Fracture", J. Am. Ceram. Soc., 38 (1) 33-37 (1955).

15 R. L. Coble and W. D. Kingery, "A Review of the Effect of Microstructure on Mechanical Behavior of Polycrystalline Ceramics", Symposium on Mechanical Behavior of Crystalline Solids, N. B. S. Monograph 59, 103-113 (1962).

16 J. White, "Some General Considerations on Thermal Shock", Trans. Brit. Ceram. Soc., 57 (10) 591-611 (1958).

17 T. L. Johnston, "Fracture Mechanisms in Crystalline Solids", Symposium on Mechanical Behavior of Crystalline Solids, N. B. S. Monograph 59, 63-78 (1962).

18 W. D. Kingery, "Note on Thermal Expansion and Microstresses in Two-Phase Compositions", J. Am. Ceram. Soc., 40 (10) 351-352 (1957).

19 P. S. Turner, "Thermal-Expansion Stresses in Reinforced Plastics", J. Res. Nat. Bur. Stand., 37 (10) 239-250 (1946).

20 S. S. Manson and R. W. Smith, "Theory of Thermal Shock Resistance of Brittle Materials Based on Weibull's Statistical Theory of Strength", J. Am. Ceram. Soc., 38 (1) 18-27 (1955).

21 W. Weibull, "Statistical Theory of Strength of Materials", Ing. Vetenskaps Akad. Hand., No. 51, (1939) 45pp.

22 A. A. Griffith, "Phenomena of Rupture and Flow in Solids", Phil. Trans. Roy. Soc. (London), A221 (4) 163-198 (1920).

23 J. Nakayama and M. Ishizuka, "Experimental Evidence for Thermal Shock Damage Resistance", Bull. Am. Ceram. Soc., 45 (7) 666-669 (1966).

24 J. Nakayama, "Direct Measurement of Fracture Energies of Brittle Heterogeneous Materials", J. Am. Ceram. Soc., 48 (11) 583-587 (1965).

25 W. C. Mohr, "Radiant Thermal Shock Testing", Bull. Am. Ceram. Soc., 44 (7) 545 (1965).

26 E. M. Baroody, E. M. Simons, and W. H. Duckworth, "Effect of Shape on Thermal Fracture", J. Am. Ceram. Soc., 38 (1) 38-43 (1955).

27 W. B. Crandall and J. Ging, "Thermal Shock Analysis

of Spherical Shapes", J. Am. Ceram. Soc., 38 (1) 44-54 (1955).

28 C. Y. King, "Internal Fracture of Glass by Thermal Shock", Doctor of Philosophy Thesis, Cornell University, (1965) 168pp.

29 E. Glenny and M. G. Royston, "Transient Thermal Stresses Promoted by Rapid Heating and Cooling of Brittle Circular Cylinders", Trans. Brit. Ceram. Soc., 57 (10) 645-677 (1958).

30 R. E. Moore, "A Statistical Analysis of Fracture Stresses of Triaxial Porcelain Bodies", Doctor of Philosophy Thesis, University of Missouri, (1962) 161pp.

31 D. P. H. Hasselman, "Tables for the Compilation of the Shear Modulus and Young's Modulus of Elasticity from the Resonant Frequencies of Rectangular Prisms", Applied Research Branch, Research and Developement Division, The Carborundum Co., Niagara Falls, New York, (1961) 195pp.

32 G. M. Smith and H. D. Berns, "Frequency-Phase Method for Measuring Material Damping", Mat. Res. Std., 4 (6) 225-227 (1964).

33 R. W. Powell, "Thermal and Electrical Conductivities of Metals and Alloys: I. Iron from 0°C to 800°C", Proc. Phys. Soc. (london), 46 (5) 659-679 (1934).

34 C. D. Coody, B. Abeles, and P. S. Beers, "Thermal Diffusivity of Armco Iron", Trans. AIME, 221 (1) 25-27 (1961).

35 M. P. Heisler, "Temperature Charts for Induction and Constant-Temperature Heating", Trans. Am. Soc. Mech. Engrs., 69 (3) 227-236 (1947).

36 W. H. Daniels and R. E. Moore, "Fracture Behavior of a Model Brittle Solid Containing Artificial Surface Flaws", J. Am. Ceram. Soc., 48 (5) 274-275 (1965).

37 A. J. Holland and W. E. S. Turner, "Effect of Transverse Scratches on the Strength of Sheet Glass", J. Soc. Glass Tech., 21 (87) 383-394 (1937).

38 A. H. Lachenbruch, "Depth and Spacing of Tension Cracks", J. Geophysical Research, 66 (12) 4273-4292 (1961).

39 A. H. Lachenbruch, "Mechanics of Thermal Contraction Cracks and Ice-Wedge Polygons in Permafrost", Special GSA Papers, No. 70, New York (1962) 68pp.

40 W. D. Kingery, J. Francl, R. L. Coble, and T. Vasilos, "Thermal Conductivity: X. Data for Several Pure Oxide Materials Corrected to Zero Porosity", J. Am. Ceram. Soc., 37 (2) 107-110 (1954).

41 Wesgo Data Sheet, Western Gold and Platinum Company, Belmont, California.

42 C. D. Pears, "Evaluation of Tensile Data for Brittle Materials Obtained with Gas Bearing Concentricity", pp. 54-58 in Air Force Materials Laboratory, Wright-Patterson Air Force Base, Ohio, Report No. ASD-TDR-63-628; Contract No. AF 33(657)-7685; May 1963.

43 N. A. Weil, "Studies of the Brittle Behavior of Ceramic Materials", p. 286 in Air Force Materials Laboratory, Wright-Patterson Air Force Base, Ohio, Report No. ASD-TR-61-628, Part II; Contract No. AF 33(616)-7465; April 1963.

44 W. H. Gitzen, "Alumina Ceramics", p. 118 in Air Force Materials Laboratory, Wright-Patterson Air Force Base, Ohio, Report No. AFML-TR-66-13; January 1966.

APPENDIX A

Letter Symbols

Symbol	Definition	Units	
		English	C.G.S.
A_i	thermal stress	Psi	dynes/cm^2
a	thermal diffusivity	in^2/sec	cm^2/sec
b	crack depth	inches	cm
C	shape constant for calculating the modulus of elasticity	in^{-2}	cm^{-2}
D	diameter	in	cm
d_i	layer of material stressed to A_i	in	cm
E	Young's modulus	Psi	dynes/cm^2
e_h, e_v	horizontal and vertical input voltages to oscilloscope	volts	volts
f, f_n	flexural frequencies of vibrating rods	cycles/sec	cycles/sec
g	gravitational constant	ft/sec^2	cm/sec^2

h	surface heat transfer coefficient	$Btu/hr/ft^2/°F$	$Cal/sec/cm^2/°C$
k	thermal conductivity	$Btu/hr/ft/°F$	$Cal/sec/cm/°C$
K	bulk modulus	Psi	$dynes/cm^2$
L	length	in	cm
LD	logarithmic decrement	dimensionless	
P	load on bars	pounds force	dynes
p_i	phase percentage	dimensionless	
q	rate of heat flow	Btu/hr	Cal/sec
R	thermal shock factor	°F	°C
r	radial coordinate	ft	cm
r^*	dimensionless radius = r/x	dimensionless	
S	shape factor	dimensionless	
T	temperature	°F	°C
T_f	fluid temperature	°F	°C
T_i	initial temperature	°F	°C
T^*	dimensionless temperature		

T* (continued)	$= \frac{T_f - T}{T_f - T_i}$	dimensionless	
t	time	hr	sec
t*	dimensionless time $= \frac{at}{R^2}$	dimensionless	
W	elastic strain energy	ft-lbs	ergs
w	weight	pounds force	dynes
x	radius	in	cm
Y_1, Y_2	vertical dimensions on oscilloscope	in	cm
α	coefficient of linear thermal expansion	/°F	/°C
β	Biot's modulus $= \frac{hR}{k}$	dimensionless	
$\Gamma(d_i/b)$	normalized stress-edge intensity factor	dimensionless	
γ	surface energy	$ft\text{-}lbs/ft^2$	$ergs/cm^2$
ΔT	temperature difference	°F	°C
ε	emissivity	dimensionless	

θ	rate of temperature rise	°F/hr	°C/sec
μ	Poisson's ratio	dimensionless	
ρ	density	lbs/ft^3	gm/cm^3
σ	tensile strength	Psi	$dynes/cm^2$
σ_r^*, σ_t^*, σ_z^*	dimensionless stresses	dimensionless	
ϕ	phase angle	radians	radians
ω	circular frequency	radians/sec	radians/sec

APPENDIX B

Stress Distribution in Long Solid Cylinders

$$\sigma_r^* = 2\beta \sum_{m=1}^{\infty} \frac{e^{-\gamma_m^2 t^*}}{(\gamma_m^2 + \beta^2) J_0(\gamma_m)} \left[\frac{J_1(r^* \gamma_m)}{r^* \gamma_m} - \frac{J_1(\gamma_m)}{\gamma_m} \right]$$

$$\sigma_t^* = 2\beta \sum_{m=1}^{\infty} \frac{e^{-\gamma_m^2 t^*}}{(\gamma_m^2 + \beta^2) J_0(\gamma_m)} \left[J_0(r^* \gamma_m) - \frac{J_1(r^* \gamma_m)}{r^* \gamma_m} - \frac{J_1(\gamma_m)}{\gamma_m} \right]$$

$$\sigma_z^* = 2\beta \sum_{m=1}^{\infty} \frac{e^{-\gamma_m^2 t^*}}{(\gamma_m^2 + \beta^2) J_0(\gamma_m)} \left[J_0(r^* \gamma_m) - \frac{2\mu J_1(\gamma_m)}{\gamma_m} \right]$$

where:

β = Biot's modulus = $\frac{hx}{k}$,

t^* = dimensionless time = $\frac{at}{x^2}$,

r^* = dimensionless radius = $\frac{r}{x}$,

μ = Poisson's ratio,

γ_m = m'th root of:

$\gamma J_1(\gamma) = \beta J_0(\gamma)$, and

a = thermal diffusivity.

APPENDIX C

Cooling Curves for Determining the Heat Transfer Coefficient

The cooling curves used to determine the surface heat transfer coefficient are given in Figure 16. Armco iron was used to obtain these cooling curves. These curves can be plotted in terms of dimensionless parameters by using the following relation:

$$T^* = \frac{T_f - T}{T_f - T_i} \tag{35}$$

$$t^* = \frac{at}{x^2}. \tag{36}$$

Figure 17 gives a plot of the cooling curves in terms of dimensionless temperature and dimensionless time. In this form, the curves can be compared with those of Heisler[35]. The dotted curves are taken from Heislers paper and correspond to reciprocal Biot's modulus values of 0.6 and 0.8. Extrapolation shows that the curve in the present case corresponds to a reciprocal Biot's modulus of 0.75. The surface heat transfer coefficient is found by the relation:

$$h = \frac{\beta k}{x}. \tag{37}$$

In the range of interest, Armco iron has an average thermal conductivity of 0.163 cal/cm/°C/sec. Therefore, using a sample having a diameter of 2.54 cm, the surface heat

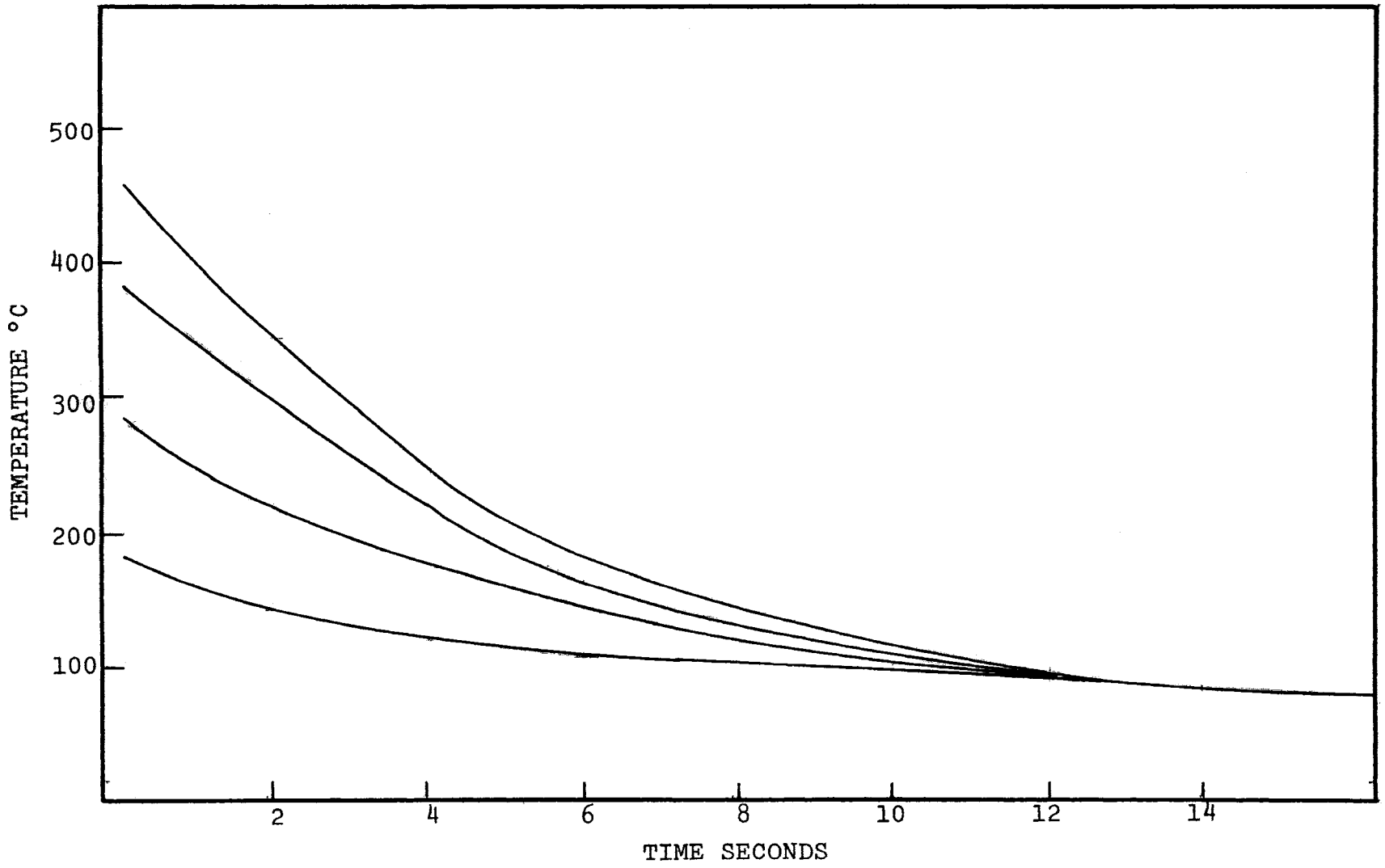

Figure 16. Cooling curves used to determine surface heat transfer coefficient.

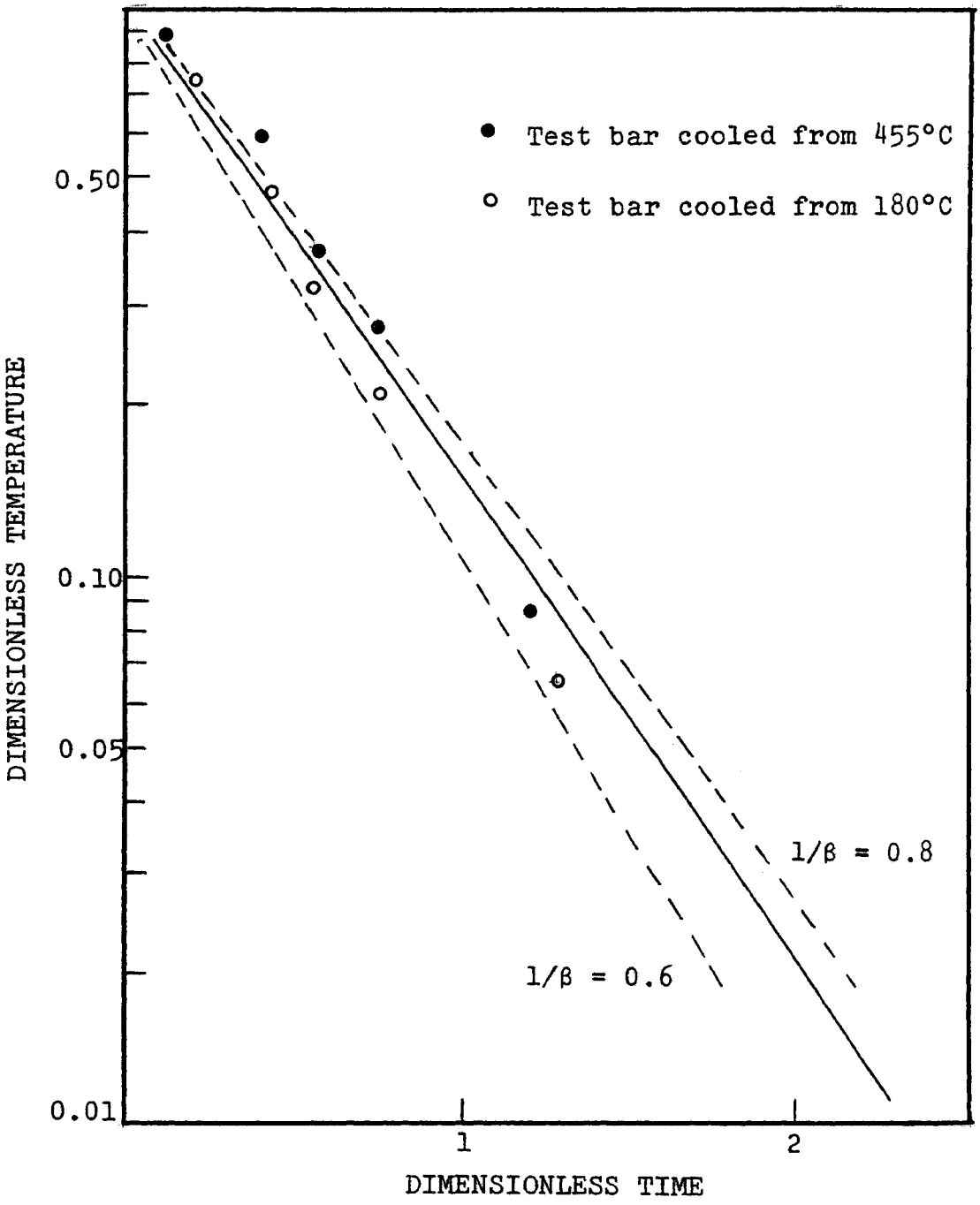

Figure 17. Cooling curves plotted in terms of dimensionless temperature and dimensionless time.

transfer coefficient is found to be:

$$h = \frac{0.163}{0.75 \times 1.27} = 0.171 \text{ cal/cm}^2/^\circ\text{C/sec.}$$

APPENDIX D

Material Properties and Sample Calculations

The purpose of this appendix is to document the properties used for all calculations in this thesis and to provide sample calculations of the data presented herein. Figures 18 through 21 give the temperature dependence of the thermal conductivity[40], thermal expansion[41], strength[42], and Young's modulus of elasticity. In addition, the following values were used for effective surface energy, Poisson's ratio, and surface heat transfer coefficient.

effective surface energy[43]....2.31 x 10^4 ergs/cm^2 ($\frac{0.132 \text{ lbs}}{\text{in}}$)

Poisson's ratio[44].....0.257

measured surface heat transfer coefficient.....

.....0.171 cal/cm^2/sec/°C.

A knowledge of the above properties allows the calculation of:

1. Thermal stress distribution within long rods.
2. Initial fracture temperature difference (ΔT_{max}).
3. Crack depths.

1. Determination of Stress Distribution Within the Long Rods

Inasmuch as Jaeger's equations are quite complex, values of the dimensionless stresses were obtained as a function of Biot's modulus, dimensionless time, and

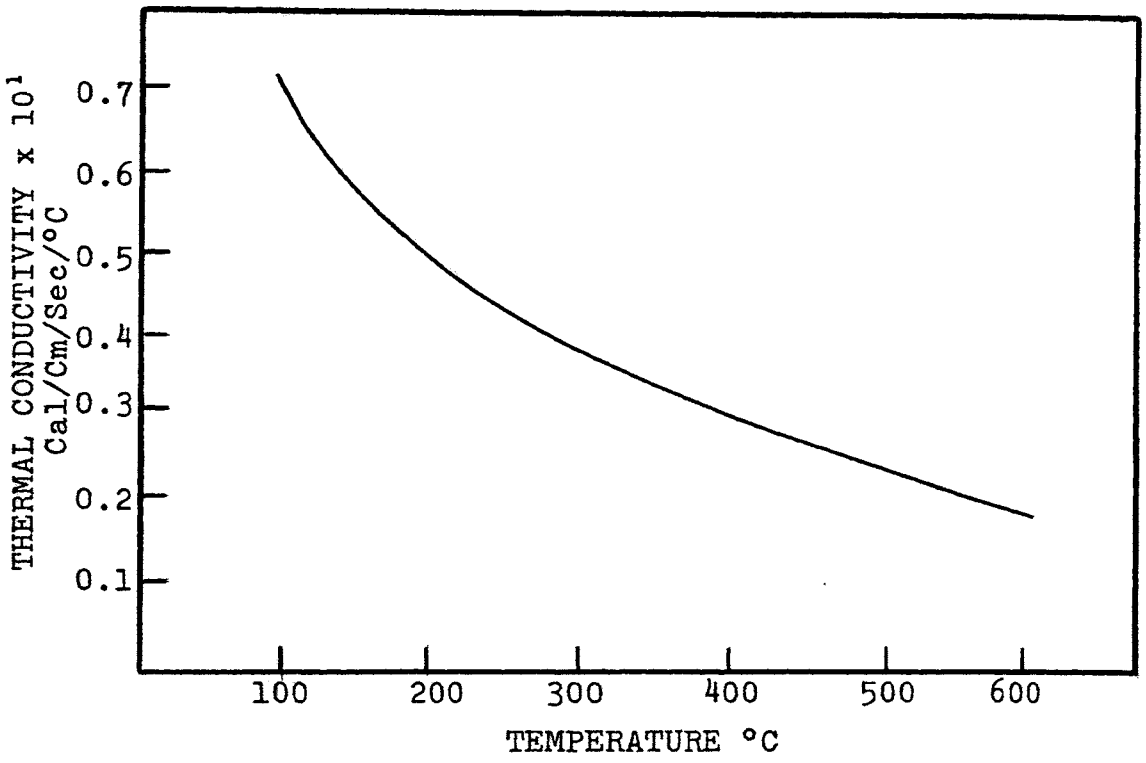

Figure 18. Thermal conductivity dependence on temperature of Al_2O_3.

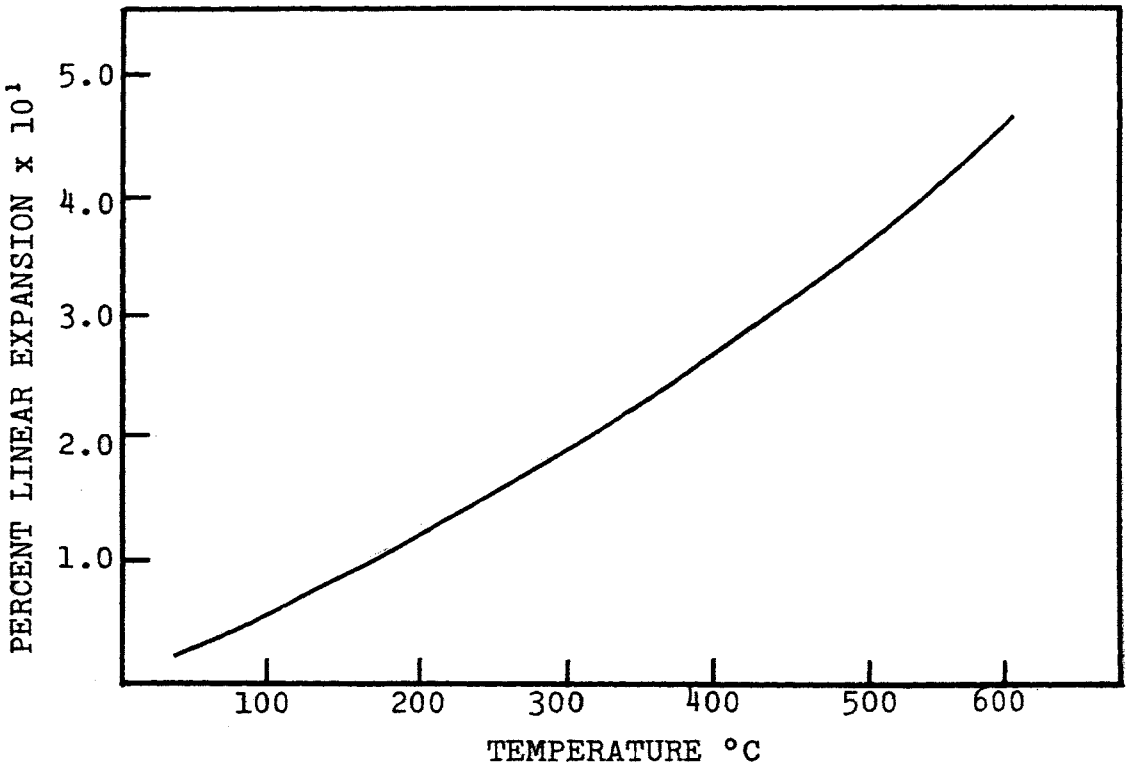

Figure 19. Thermal expansion of Al_2O_3.

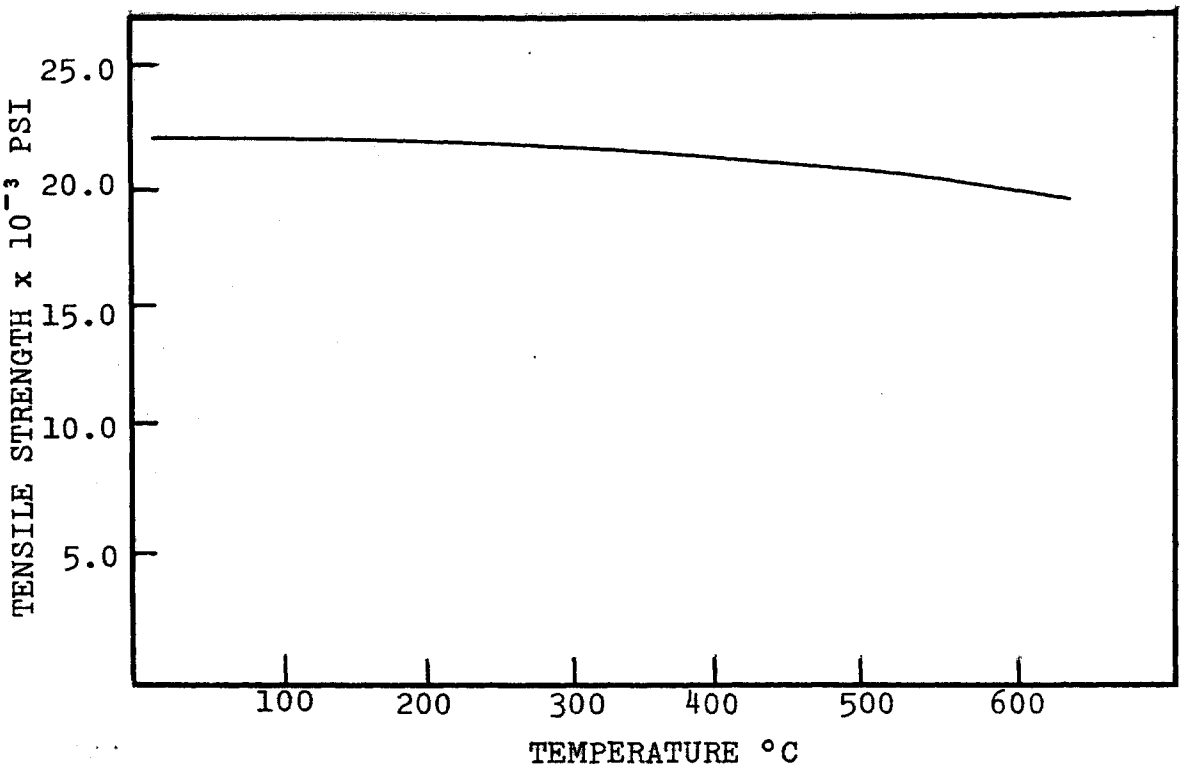

Figure 20. Temperature dependence of strength of Al_2O_3.

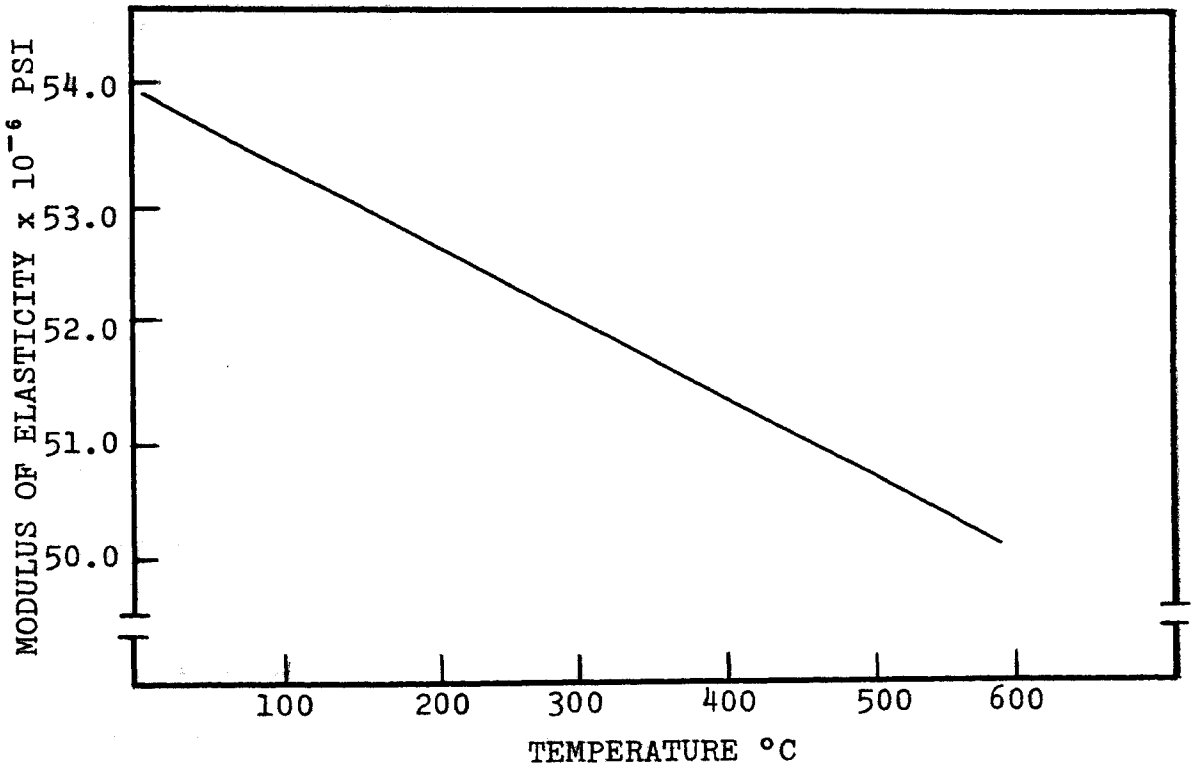

Figure 21. Temperature dependence of Young's modulus of Al_2O_3.

dimensionless radial coordinates with the aid of a computer. Table VIII gives these stresses for selected values of the dimensionless parameters above.

2. Determination of ΔT_{max}

The properties which affect the calculated value of ΔT_{max} are temperature dependent. The problem is, thus, the temperature at which to evaluate these material properties. Kingery[4] suggests evaluating the material properties at a temperature defined by the relation:

$$T = 0.8\ \Delta T_{max}. \tag{38}$$

ΔT_{max} is calculated from the relation:

$$\Delta T_{max} = \frac{\sigma(1 - \mu)}{E\alpha\sigma_t^*}. \tag{39}$$

Figure 22 shows how the calculated ΔT_{max} value varies with the temperature at which the material properties are evaluated. Also shown in Figure 22 is a plot of equation 38. The intersection of these two curves gives the required value for ΔT_{max}. Table IX gives the material properties as a function of temperature as well as the calculated ΔT_{max} values evaluated at those temperatures. Figure 22 shows that the required value of ΔT_{max} is 184°C.

3. Calculation of Crack Depth

Figure 14 indicates that the modified Lachenbruch equation (equation 34) employs discrete stress increments to approximate the continuous stress distribution given by Jaeger's equations. To calculate the crack depths, the

TABLE VIII

Dimensionless Tangential Stresses at the Time of Maximum Stress as a Function of Dimensionless Radial Coordinates and Biot's Modulus

Dimensionless Radial Coordinates	$\beta = 1.5$	$\beta = 1.85$	$\beta = 2.0$	$\beta = 2.8$	$\beta = 3.6$
1.00	0.216	0.234	0.247	0.298	0.337
0.90	0.146	0.138	0.165	0.195	0.215
0.80	0.084	0.087	0.093	0.107	0.112
0.70	0.034	0.034	0.035	0.037	0.033
0.60	-0.005	-0.009	-0.009	-0.015	-0.024
0.50	-0.035	-0.038	-0.041	-0.051	-0.061
0.40	-0.056	-0.059	-0.063	-0.075	-0.083
0.30	-0.069	-0.072	-0.077	-0.089	-0.095
0.20	-0.078	-0.082	-0.085	-0.097	-0.101
0.10	-0.083	-0.086	-0.089	-0.101	-0.104

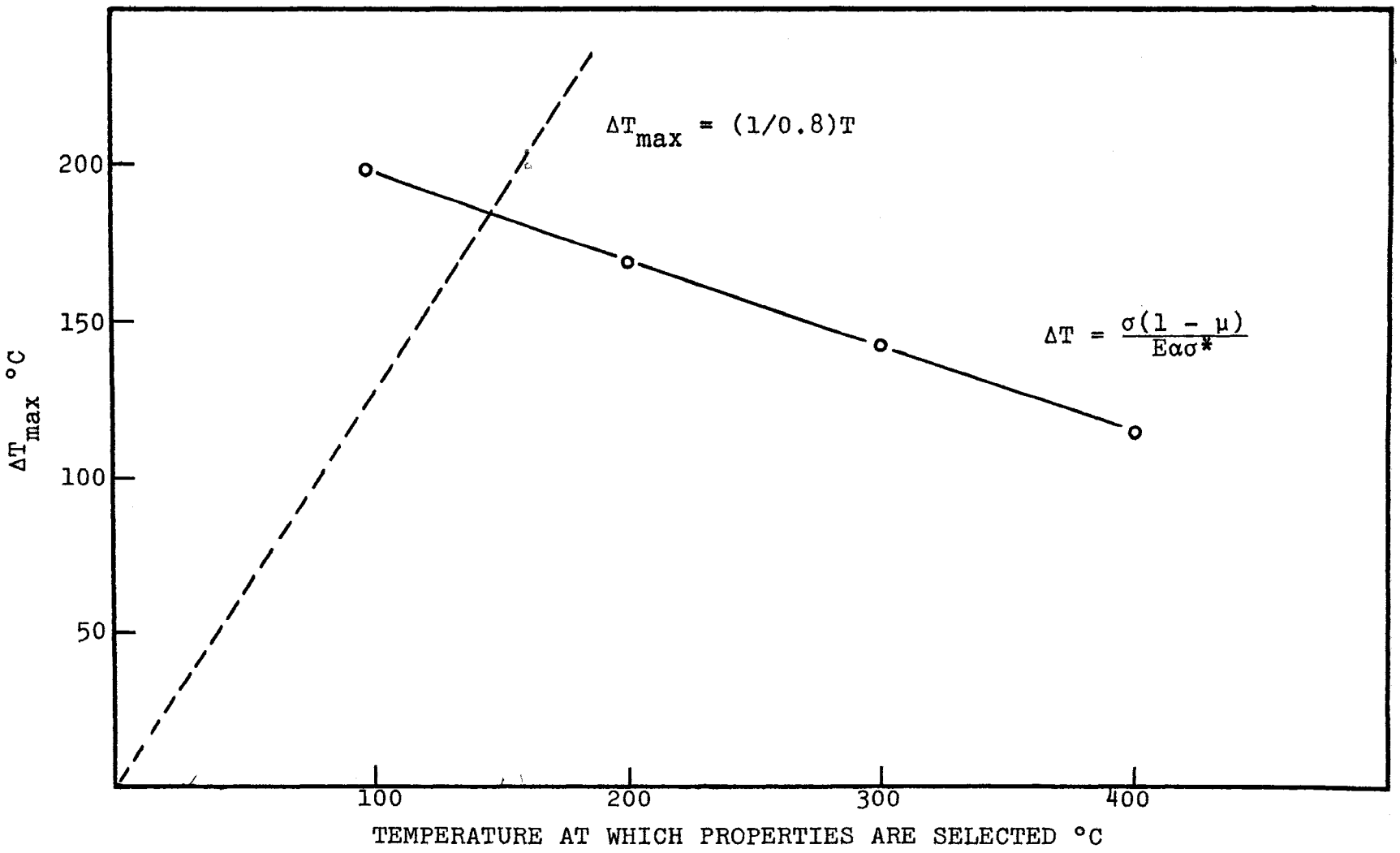

Figure 22. The effect of property evaluation temperature on the calculated ΔT_{max}.

TABLE IX

Effects of Property Evaluation Temperature on Calculated ΔT_{max}

Property Evaluation Temperature (°C)	Tensile Strength (Psi)	Young's Modulus (x 10^{-6} Psi)	Thermal Conductivity (Cal/Cm/°C/Sec)	Thermal Expansion (x 10^{6} °C^{-1})
100	21,800	53.4	0.073	7.2
200	21,800	52.6	0.054	7.3
300	21,700	52.0	0.040	7.5
400	21,600	51.4	0.030	7.9

Property Evaluation Temperature (°C)	Poisson's Ratio	Biot's Modulus	Maximum Dimensionless Stress at Surface	Calculated ΔT_{max} (°C)
100	0.26	1.5	0.216	195
200	0.26	2.0	0.247	170
300	0.26	2.8	0.297	139
400	0.26	3.6	0.338	117

stress increments d_i have been chosen such that:

$$d_1 = d_2 = \ldots\ldots = d_n = 0.05x, \tag{40}$$

where x = radius.

Thus, equation 34 may be arranged and written as:

$$b = 0.016x^2 \ (\Sigma A_i)^2 \ \frac{(1 - \mu^2)\pi}{E\gamma}. \tag{41}$$

Inspection of equation 40 reveals that there are effectively two unknowns: the crack depth b and the number of discrete stress summations needed to correspond to the crack depth. If too many summations are employed, the calculated crack depth will be too small. If, on the other hand, too few summations are used, the calculated crack depth will be too large. In the present case, each successive stress summation is made at a point which corresponds to a greater depth within the specimen. It is necessary to match the final depth to which stresses are summed with the calculated crack depth value b which this summation yields.

A graphical solution has been devised to obtain the correct values for the crack depths. This method involves plotting calculated crack depths for successive stress summations against the radial coordinate corresponding to the depths to which the summations are made. Also plotted are values of crack depths which correspond directly to the radial coordinates. This plot is a straight line. These two plots intersect at a point which corresponds

to the correct value for the calculated crack depth. Table X gives the calculations necessary to plot these curves for the crack depths corresponding to a 175°C ΔT.

The discrete stresses A_i are calculated using equation 39, and the crack depths b are calculated using equation 41. The dimensionless tangential stresses were calculated as described in section 1 of this appendix. Figure 23 shows these plots and how the correct crack depth value is obtained.

TABLE X

Calculations for Tangential Crack Depths Resulting From 175°C ΔT Shock

Radial Coordinate	Depth in Specimen (Inches)	Dimensionless Stress (σ^*)	Mean Dimensionless Stress	A_i (Psi)	ΣA_i (Psi)	Calculated Crack Depth (Inches)
1.00	0	0.234				
			0.210	18,800	18,800	0.148
0.95	0.013	0.186				
			0.162	14,500	33,300	0.465
0.90	0.025	0.138				
			0.126	11,300	44,600	0.836
0.85	0.038	0.113				
			0.100	8,950	53,550	1.21
0.80	0.050	0.087				
			0.074	6,620	60,170	1.52
0.75	0.063	0.060				
			0.047	4,210	64,380	1.74
0.70	0.075	0.034				
			0.023	2,060	66,440	1.84
0.65	0.088	0.012				
			0.001	90	66,530	1.86
0.60	0.10	-0.009				
			-0.016	-1,430	65,100	1.78
0.55	0.113	-0.022				
			-0.030	-2,680	62,420	1.63
0.50	0.125	-0.038				
			-0.043	-3,850	58,570	1.45
0.45	0.138	-0.048				
			-0.054	-4,840	53,730	1.22

TABLE X (Continued)

0.40	0.150	-0.059	-0.063	-5,650	48,080	0.970
0.35	0.163	-0.066	-0.069	-6,190	41,890	0.738
0.30	0.175	-0.072	-0.074	-6,620	35,270	0.524
0.25	0.188	-0.076	-0.078	-6,980	28,380	0.337
0.20	0.200	-0.080	-0.081	-7,250	21,130	0.198
0.15	0.213	-0.082	-0.083	-7,420	13,710	0.079
0.10	0.255	-0.084	-0.085	-7,610	6,100	0.016
0.05	0.238	-0.05	-	-	-	-

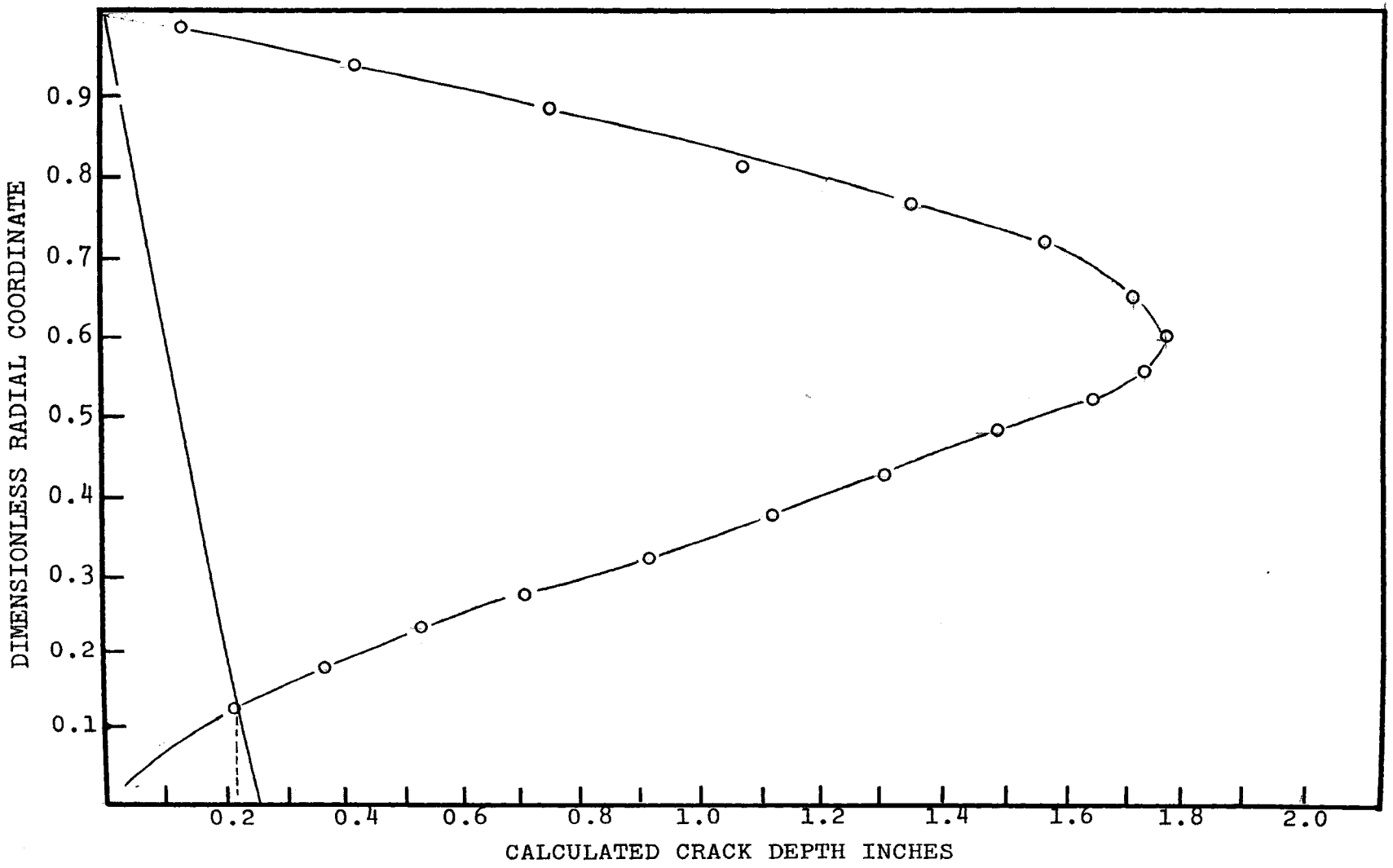

Figure 23. Graphical method for calculating crack depths.

VITA

John Homer Ainsworth was born in McKeesport, Pennsylvania on July 12, 1941. After receiving elementary school training at the Delmont public school, Delmont, Pennsylvania, he attended Greensburg High School in Greensburg, Pennsylvania and Franklin Area Joint High School in Newlonsburg, Pennsylvania. He graduated from Franklin Area Joint High School in May 1959.

In September 1959, he entered the University of Missouri, School of Mines and Metallurgy where he studied Ceramic Engineering. He received the Bachelor of Science Degree in Ceramic Engineering in May 1963.

From June 1963 to June 1964 he worked as a research engineer in the Technical Center at Ferro Corporation in Cleveland, Ohio.

In June 1964 he entered the Graduate School of the University of Missouri at Rolla. He received the Master of Science from that school in May 1966. He remained at the University of Missouri at Rolla until February 1968 to work on a Ph. D. in Ceramic Engineering.

He is currently employed as a research engineer by the Babcock and Wilcox Company in Alliance, Ohio.

He is a member of the American Ceramic Society and Keramos.